이학박사 학위논문

Spatial Arrangement of Quantum Dots Directed by Nanostructures of Block Copolymers

블록공중합체 나노구조에 의한 양자점의 배열에 관한 연구

2016년 8월

서울대학교 대학원

화학부 고분자화학

채 승 용

Abstract

Spatial Arrangement of Quantum Dots Directed by Nanostructures of Block Copolymers

Seungyong Chae

Department of Chemistry

The Graduate School

Seoul National University

Metal, oxide, and semiconductor nanoparticles have attracted considerable attention due to their unique properties, which are different from those of their respective bulk materials. Advances in the synthesis of spherical nanoparticles with uniform size have also made it possible to extend this difference by creating ensembles of nanoparticles within assemblies in solution or solids. Single and

binary crystal structures of nanoparticles with long-range order over hundreds of microns have already been achieved using this approach; thus, considerable effort is now being directed toward going beyond these close-packed structures to produce tailored structures of spatially arranged nanoparticles. Such an arrangement can be obtained using "top-down" techniques such as e-beam and photo lithography; however, conventional lithographic techniques are only effective with solids on a substrate. In contrast, "bottom-up" self-assembly provides a platform for generating 1-D, 2-D, and 3-D ordered arrays. Here, block copolymers composed of two or more chemically different polymers provide an ideal template for directing the arrangement of nanoparticles, as they have a self-assembled nanostructure over macroscopic distances in solid and solution.

In this thesis, we focus on the directed spatial arrangement of quantum dots (QDs) by block copolymer nanostructures, which requires selective compatibility between the two. To this end, we introduced functionalities into specific copolymer blocks or QDs to improve their interaction, thereby allowing QDs to be arranged along the nanostructure of a block copolymer in a composite film, or encapsulated and linearly arranged by block copolymer micelles in solution. Furthermore, by combining organic fluorophores with different kinds of QDs, multiple-fluorescence controlled by the nanostructure of the block copolymer was achieved.

Chapter 1 gives a brief overview of the nanostructure of block copolymers when self-assembled in a solid and in solution. The synthesis and post-polymerization modification of block copolymers for functionalization is also introduced.

In Chapter 2, we demonstrate that the spatial arrangement of QDs can be directed by the lamellar nanostructure of a functional block copolymer in a composite film. As it is the polymer matrix that directs the arrangement of QDs, post-polymerization modification is used to create a diblock copolymer containing a reactive block with thiol functionalities that can interact with QDs. Thin films of this block copolymer are fabricated with various thicknesses by spin-coating, with solvent annealing being used to create perpendicular and parallel lamellar nanostructures for the selective arrangement of QDs. A free-standing film with a randomly orientated lamellar nanostructure is also fabricated by solvent-casting, comparison with which reveals that the absorbance and photo luminescent properties of the QDs are preserved in all of the composite films.

In Chapter 3, we describe how the simultaneous arrangement of two fluorophores is achieved using the nanostructure of a block copolymer by blending the thiol-functionalized block copolymer used in Chapter 2 with an organic fluorophore-anchored block copolymer. This has the same basic chemical structure for each block, but has slightly different functional moieties in one of

its blocks so that it can be incorporated into the same nanostructure. Organic fluorophores are also introduced along the reactive block using the post-polymerization modification method demonstrated in Chapter 2, producing a lamellar nanostructures was also confirmed. Thus, functionalized block copolymers, QDs and organic fluorophores are all simultaneously arranged into the lamellar nanostructure of a block copolymer. Fluorescence resonance energy transfer (FRET) is observed between the QDs and organic fluorophores which were concurrently confined in the nanoscale domains.

The linear arrangement of QDs under the direction of the supracolloidal polymer chain of a block copolymer micelle in solution is presented in Chapter 4. Here, we encapsulated green- or red-emitting QDs in the diblock copolymer micelles which have cross-linked core, and then induced supracolloidal polymer chains by sequentially changing the polarity of the solvent. Since each chain contained ether green- or red-emitting QDs, fluorescent supracolloidal chains functionalized with QDs were successfully produced. Furthermore, by combining the micellar monomers into monomeric and polymeric states, we were able to achieve supracolloidal random and block chains with green and red emissions, as observed directly by structured illumination microscopy.

Keywords : Diblock Copolymer, Self-assembly, Quantum Dot, Templated Arrangement, Supracolloidal Polymer

Student Number : 2008-22739

Contents

Abstract 1

Contents 6

List of Figures 8

Chapter I. Introduction 12

1.1 Motivation 13

1.2 Nanostructures of Block Copolymers 17

1.3 Synthesis and Post-polymerization Modification of Block Copolymers 20

1.4 References 23

Chapter II. Spatial Arrangement of Quantum Dots Directed by Block Copolymer Lamellar Nanostructures in Composite Films 30

2.1 Introduction 31

2.2 Experimental Section 33

2.3 Results and discussion 36

2.4 Conclusion 41

2.5 References..... 42

Chapter III. Simultaneous Incorporation of Dual Fluorophores into Nanostructures of Functional Block Copolymers..... 50

3.1 Introduction..... 51

3.2 Experimental..... 53

3.3 Results and discussion..... 55

3.4 Conclusions..... 60

3.5 References..... 61

Chapter IV. Fluorescent Supracolloidal Polymer Chains of Quantum Dots Encapsulated by Diblock Copolymer Micelle..... 68

4.1 Introduction..... 69

4.2 Experimental..... 72

4.3 Results and discussion..... 76

4.4 Conclusions..... 85

4.5 References..... 86

Abstract in Korean..... 102

List of Figures

Chapter II

Figure 2-1. CdSe@ZnS QDs: (a) TEM image; (b) PL spectrum. The scale bar in the image is 100 nm. The excitation wavelength for the PL was 360 nm.

Figure 2-2. Synthetic schemes: (a) RAFT Polymerization of PMMA-PPFPMA; (b) Thiol-functionalization of PMMA-PPFPMA

Figure 2-3. TEM images of thin films with perpendicularly oriented lamellar nanostructures: (a) PMMA-PPFPMA; (b) mixture of PMMA-P(PFPMA-SH) and QDs. Cross-sectional TEM images of thin film with parallel oriented lamellar nanostructures: (c) PMMA-PPFPMA; (d) mixture of PMMA-P(PFPMA-SH) and QDs, The scale bars in the images are 100 nm.

Figure 2-4. PL Spectrum of thin films of PMMA-P(PFPMA-SH) with QDs. The excitation wavelength for the PL was 360 nm.

Figure 2-5. Cross-sectional TEM images of casted films: (c) PMMA-PPFPMA; (d) mixture of PMMA-P(PFPMA-SH) and QDs, The scale bars in the images are 100 nm.

Chapter III

Figure 3-1. Synthetic scheme: fluorophore functionalization of PMMA-PPFPMA

Figure 3-2. ^{1}H NMR of PMMA-P(PFPMA-SH) in CD_2Cl_2

Figure 3-3. Schematic illustration of lamellar nanostructures in a thin film of PMMA-P(PFPMA-TAMRA) (left), cross-sectional TEM image (center) and PL spectrum of the film (right). The excitation wavelength was 360 nm.-

Figure 3-4. UV-Vis spectra of the solutions used for spin coating of thin films of block copolymers: only with QDs (green dashed line); only with TAMRA (red dashed line); with both QDs and TAMRA (pink solid line).

Figure 3-5 Schematic illustration (left), cross-sectional TEM image (center), and PL spectrum (right) of a thin film consisting of QDs, PMMA-P(PFPMA-SH), and PMMA-P(PFPMA-TAMRA). The scale bar in the image is 100 nm. The excitation wavelength for the PL was 360 nm. PL spectra of thin films only with QDs (green dashed line) and only with TAMRA (red dashed line) are displayed together.

Chapter IV

Figure 4-1. UV-Vis (dashed) and photoluminescence (solid) spectra of green QDs (green) and red QDs (red).

Figure 4-2. TEM Images: (a) green QDs; (b) spherical micelles with green QDs; (c) red QDs; (d) spherical micelles with red QDs. All scale bars are 50 nm.

Figure 4-3. Dynamic light scattering (DLS) results of PS-b-P4VP micelles with QDs: (a) micelles with green QDs; (b) micelles with red QDs.

Figure 4-4. Histograms of the number of QDs per micelle: (a) green QDs; (b) red QDs.

Figure 4-5 TEM images of patched micelles with green QDs (a,b), and with red QDs (c,d). Left images (a,c) were stained with I_2 whereas right images were stained with RuO_4. All scale bars are 100 nm.

Figure 4-6 Supracolloidal chains functionalized with green QDs (top row) and red QDs (bottom row): (a)(d) TEM images; (b)(e) PL spectra with photos; (c)(f) SIM images. TEM images correspond to the marked areas in the insets showing whole chains. The scale bars in TEM and SIM images are 100 nm and 1 μm, respectively.

Figure 4-7 TEM image of a supracolloidal polymer chain with green QDs shown in the inset of Figure 4-6a. The scale bar is 500 nm.

Figure 4-8 Large-area SIM image of supracolloidal chains functionalized with green QDs. The scale bar is 1 μm.

Figure 4-9 TEM image of a supracolloidal polymer chain with red QDs shown in the inset of Figure 4-6(d). The scale bar is 500 nm.

Figure 4-10 Large-area SIM image of supracolloidal chains functionalized with red QDs. The scale bar is 1 μm.

Figure 4-11 Supracolloidal random (top row) and block (bottom row) copolymer chains functionalized with green QDs and red QDs: (a)(d) TEM images; (b)(e) PL spectra with photos; (c)(f) SIM images. TEM images correspond to the marked areas in the insets showing whole chains. Green and red false colors are applied to the cores containing green and red QDs, respectively. The scale

bars in TEM and SIM images are 100 nm and 1 μm, respectively.

Figure 4-12 TEM image of a supracolloidal random copolymer chain with green and red QDs shown in the inset of Figure 4-11(a). Green and red false colors are applied to the cores containing green and red QDs, respectively. The scale bar is 500 nm.

Figure 4-13 TEM image of a supracolloidal block copolymer chain with green and red QDs shown in the inset of Figure 4-11(d). Green and red false colors are applied to the cores containing green and red QDs, respectively. The scale bar is 500 nm.

Chapter I.

Introduction

1-1.Motivation

Metal, oxide and semiconductor nanoparticles have attracted considerable attention due to their unique properties which are different from the properties in their bulk materials.[1] Especially, some of their properties are due to quantum confinement effects depending on their sizes and shapes.[2,3] For example, Semiconductor nanocrystals, often called quantum dots (QDs), have excellent fluorescent properties with unique features such as high resistance to photo bleaching and broad absorption, narrow emission spectra, high luminescence efficiency in the solid state and tunability over a wide emission wavelength range.[4] Metallic nanoparticles have localized surface plasmon resonance which is promising for next-generation optical and sensing.[5]

Advances in the synthetic methods for nanoparticles with uniform sizes and shapes have enabled the effective construction of their assemblies in the solid and solution state.[6-10] Different properties can be derived from ensembles of nanoparticles inside these assemblies.[11] Single and binary crystal structures of nanoparticles with long-range order over hundreds of microns have already been achieved using this approach.[7-9]

Beyond these close-packed structures, many efforts have been devoted into tailored structures of spatially arranged nanoparticles.[12-16] These arrangement

can be obtained using “top-down” techniques such as e-beam and photo lithography.[12,13] However, conventional lithographic techniques are effective in solid states on substrate. On the other hand, “bottom-up” self-assembly approaches provide platforms to generate 1-D, 2-D and 3-D ordered arrays.[14] To achieve the desired structures, strong directional forces are needed for directing the aggregation process.[15] Chemical interactions of ligand shells including electrostatic or hydrophobic interactions were utilized.[16] External field such as electric or magnetic fields were also used to direct the assemblies of nanoparticles.[17]

Guiding method using predefined templates which have specific reactive sites also widely used to arrange nanoparticles.[14] DNA linkers, carbon nanotubes or polymeric objects are considered as templates to direct the arrangements of nanoparticles. Especially, DNA can provide precise control of multi-dimensional assembled structure and their inter-particle distance.[18] However, arrangements of nanoparticles using DNA are not suitable for device fabrication because of their high cost. In this point of view, block copolymers which is composed of two or more chemically different polymers can be an alternative candidate as a templates for the directing arrangement of nanoparticles due to their self-assembled nanostructures over macroscopic distances in solid and solution states.[1,19,20]

Two major strategies have been studied to fabricate nanoparticle arrays within

block copolymer nanostructures: *in situ* synthesis of nanoparticles and *ex situ* incorporation of preformed nanoparticles.[21] For *in situ* nanoparticle synthesis, inorganic precursors can be incorporated in selective block then can be tuned into particles *via* reduction process. Well-ordered arrays of nanoparticles were generated in bulk and thin film with lamellar and cylinder nanostructure and single layered hexagonal array of spherical micelle.[22-24] This *in situ* synthesis is widely used for various application because of it is easy to implement. But it is not applicable for some of nanoparticle such as metallic nanorods or QDs.

On the other hand, the arrangement of preformed nanoparticles by incorporating them into block copolymer nanostructures has been extensively studied.[25-38] The co-assembled structures of nanoparticles with block copolymers result from a delicate energy balance of the enthalpic contribution, controlled by the interaction between the surface of nanoparticles and the segments of the block copolymers, and the entropic contribution based on the chain stretching penalty for accommodating nanoparticles.[25] For arrangement of nanoparticles in selective nanodomain of copolymers, the surface of nanoparticles are usually identical or similar to one of the blocks to give enthalpic contribution rely on weak van der Waals interactions.[26-33] To achieve stronger selective incorporation of nanoparticles with well-ordered nanostructures, it is needed either to make the enthalpy favorable or to relieve the entropic penalties

due to incorporation of nanoparticles. To achieve former condition, strong enthalpic interactions such as ionic interaction, dipole-dipole interaction, hydrogen bonding were introduced between the one block of copolymer and the nanoparticles.[34-37] With the latter approach, coil-comb architecture reducing the entropic penalty for nanoparticle incorporation was induced by supramolecular assemblies with small molecules, and various kinds of nanoparticles of different sizes were effectively sequestered in the center of nanodomain.[25,38]

In this thesis, we focus on the directed spatial arrangement of QDs by block copolymer nanostructures, which requires selective compatibility between the two. To this end, we introduced functionalities into specific copolymer blocks or QDs to improve their interaction, thereby allowing QDs to be arranged along the nanostructure of a block copolymer in a composite film, or encapsulated and linearly arranged by block copolymer micelles in solution. Furthermore, by combining organic fluorophores with different kinds of QDs, multiple-fluorescence controlled by the nanostructure of the block copolymer was achieved.

1-2. Nanostructures of Block Copolymers

Block copolymers consisting of two or more chemically distinct and immiscible polymer blocks that are covalently linked together spontaneously self-assemble into ordered nanostructures on the tens of nanometer scale.[39,40] For example, linear diblock copolymers which is the simplest can micro-phase separate into a various morphologies such as spheres, cylinders, bicontinuous gyroids, perforated layers, modulated lamellae and lamellae due to an unfavorable mixing enthalpy coupled with a small mixing entropy and the covalent bond connecting two blocks preventing macro-phase separation. [39]

Block Copolymers in Bulk

The size and morphology of micro-separated structures of AB diblock copolymers is determined by the three parameters: (1) the volume fractions of the A and B blocks (f_A, f_B); (2) the Flory-Huggins parameter, χ_{AB}; (3) the degree of polymerization (N). The χ_{AB} parameter reflecting the degree of incompatibility between the A and B blocks, is inversely proportional to temperature.[41,42] For diblock copolymers which has no strong specific interactions like ionic charges or hydrogen bonding, χ_{AB} is generally positive and small.

At equilibrium the nanostructures of block copolymers are controlled by

delicate balance between the entropic and the enthalpic energy contribution to minimize the overall free energy.[39] The magnitude of the entropic energy contribution is largely determined by the degree of polymerization, *N*, while that of enthalpic energy contribution is controlled predominantly by χ_{AB}. So that the product of them, χN, is used to parameterize theoretically block copolymer phase behavior, along with the composition of A block in copolymer, f_a.[42]

Block Copolymer in Thin Film

In diblock copolymer thin films which have thickness of less than 100 nm, the self-assembly process is strongly influenced by the interface energetics (e.g., polymer-substrate, and polymer-air interface).[43] When a thin film of a diblock copolymers on a strongly preferential surface is thermally annealed over the glass transition temperature (T_g) of both blocks, in-plane microdomains in copolymer films evolve.[44] In contrast, provided that the surface of a substrate is modified such that the interfacial energy is identical for both blocks, the microdomains are aligned perpendicular to the substrate.[45,46] And in thin films, confinement with film thickness significantly influence to the morphologies and the domain spacing.[47] Because stretching or compression of polymer chains due to confinement is energetically unfavorable, block copolymers self-assemble into morphologies that relieve the stretching/compression or mitigate the entropic

penalty with favorable enthalpic interactions at the interfaces.[43]

Block Copolymers in Solution

In a selective solvent for B blocks, amphiphilic AB diblock copolymers form micelles consisting of a insoluble A core and a soluble B corona.[48] Depending on the sizes of core and corona, two kind of model, "crew-cut micelle" and "hairy micelle", were introduced. For "crew-cut micelle", the core is much larger than the corona ($N_A >> N_B$). Whereas for "hairy micelle", the corona is much larger than the core ($N_A << N_B$).[49,50]

Amphiphilic AB diblock copolymers are characterized by large interaction parameters χ. If $\chi = \chi_{AB} \approx \chi_{AS} >> \chi_{BS}$ (S = solvent), then χN can serve as a parameter to characterize their thermodynamic state. Where $\chi N >> 10$ (strong segregation), the core contains practically only A blocks, the B domain is swollen with solvent, and practically no block copolymers are in solvent phase, that means the micellization is occurred.[50]

Paralleling block copolymer self-assembly in bulk, copolymer composition also affects the self-assembly in solution. As the volume ratio of the soluble B block deceases, various morphologies of AB diblock copolymer micelles are possible from spheres, through cylinders and vesicles, to LCMs, The overall

structure may be due to the high content of the block copolymer in the insoluble part, to the block copolymer architecture, and also to the selectivity of the solvent.[51]

1-3. Synthesis and Post-polymerization Modification of Block Copolymers

Reversible Addition-Fragmentation Chain Transfer (RAFT) Polymerization

To obtain well-defined nanostructures of block copolymers, preparing block copolymers with precisely designed molecular architectures is essential.[40] In the chain-growth polymerization with living manner which can be described fast initiation and no termination, block copolymer can be synthesized through sequential polymerization of each blocks.[52] Living anionic polymerization was the first and only example of a living process for more than a decade after its realization.[53] The advent of controlled radical polymerization (CRP) initiated nitroxide mediated polymerization (NMP)[54] and furthered through the development of atom transfer radical polymerization (ATRP)[55] and reversible addition fragmentation chain transfer (RAFT)[56], has enlarged the possibility of molecular weight control to a wide variety of monomers which could not be polymerized by conventional anionic polymerization. The essence of a CRP

process is fast and adjustable equilibria between active and dormant species of propagating polymer radicals.[52] In the RAFT polymerization, for example, reversible deactivation can be occurred by chain transfer facilitated thiocarbonylthio functionalities.[56] RAFT polymerization is arguably the most versatile of the reversible deactivation radical polymerization processes, with most monomers that polymerize radically able to be controlled via the RAFT process. RAFT controls the polymerization of a broader range of functional monomers than do competing techniques, providing good control over the polymerization of vinyl esters (e.g. vinyl acetate) and vinylamides (e.g. N-vinylpyrrolidone), where NMP and ATRP typically provide minimal control.[57] Additionally, RAFT is compatible with a wide variety of reaction media, being routinely applied in organic solution, aqueous solution and in dispersed phase.[58]

Post-polymerization Modification

Recently, the demands of functional polymers that are specifically designed are rapidly growing in material science for specialized applications.[59] Despite the tremendous progress in the area of controlled polymerization techniques, direct polymerization often suffers from a limited functional group tolerance under the polymerization condition. However, it can be an effective approach that polymers are modified the reactive site with the desired function after

polymerization. It is referred to as post-polymerization modification. [59] Since Sharpless and coworkers introduced the concept of ‘‘click’’ chemistry in 2001,[60] various reactive groups such as aldehyde,[61] azide,[62] and activated ester[63-65] have been applied for the functionalization of polymers by post-polymerization modification. More functional groups employed in poly-polymerization reactions are explained in the review article.[66, 67]

Particularly, vinyl monomers with an activated ester like pentafluorophenyl(meth)acrylate can be polymerized by RAFT polymerization with a narrow distribution of molecular weights.[68,69] The synthesized polymers with activated esters can be easily modified with good reactivity and are soluble in organic solvents.[64] For example, block copolymers containing activated esters were synthesized and modified for bio-compatible or stimulus-responsible micelles,[70,71] and surface alteration of metal oxide nanorods or QDs.[72-74]

1-4. References

[1] A. Haryono, W. H. Binder, *Small*, **2006**, *2*, 600.

[2] C. L. Choi, A. P. Alivisatos, *Annu. Rev. Phys. Chem.*, **2010**, *61*, 369.

[3] D. V. Talapin, J.-S. Lee, M. V. Kovalenko, E. V. Shevchenko, *Chem. Rev.*, **2010**, *110*, 389.

[4] Y. Shirasaki, G. J. Supran, M. G. Bawendi, V. Bulovic, *Nat. Photonics*, **2013**, *7*, 13.

[5] E. Hutter, J. H. Fendler, *Adv. Mater.*, **2004**, *16*, 1685.

[6] C. B. Murray, C. R. Kagan, M. G. Bawendi, *Annu. Rev. Mater. Sci.*, **2000**, *30*, 545.

[7] D. Vanmaekelbergh, *Nano Today*, **2011**, *6*, 419.

[8] Z. Chen, J. Moore, G. Radtke, H. Sirringhaus, S. O'Brien, *J. Am. Chem. Soc.*, **2007**, *129*, 15702.

[9] C. B. Murray, C. R. Kagan, M. G. Bawendi, *Science*, **1995**, *270*, 1335.

[10] C. R. Kagan, C. B. Murray, *Nat. Nanotechnol.*, **2015**, *10*, 1013.

[11] Z. H. Nie, A. Petukhova, E. Kumacheva, *Nat. Nanotechnol.*, **2010**, *5*, 15.

[12] J. Y. Cheng, C. A. Ross, V. Z. H. Chan, E. L. Thomas, R. G. H. Lammertink,

G. J. Vancso, *Adv. Mater.*, **2001**, *13*, 1174.

[13] X. Y. Ling, I. Y. Phang, W. Maijenburg, H. Schonherr, D. N. Reinhoudt, G. J. Vancso, J. Huskens, *Angew. Chem., Int. Ed.*, **2009**, *48*, 983.

[14] M. Grzelczak, J. Vermant, E. M. Furst, L. M. Liz-Marzán, *ACS Nano*, **2010**, *4*, 3591.

[15] L. J. Hill, N. Pinna, K. Char, J. Pyun, *Prog. Polym. Sci.*, **2015**, *40*, 85.

[16] F. Westerlund, T. Bjørnholm, *Curr. Op. Colloid Interface. Sci.*, **2009**, *14*, 126.

[17] J. Vermant, M. J. Solomon, *J. Phys.: Condens. Matter*, **2005**, *17*, R187.

[18] S. J. Barrow, A. M. Funston, X. Wei, P. Mulvaney, *Nano Today*, **2013**, *8*, 138.

[19] S. Darling, *Prog. Polym. Sci.*, **2007**, *32*, 1152.

[20] J. Kao, K. Thorkelsson, P. Bai, B. J. Rancatore, T. Xu, *Chem. Soc. Rev.*, **2013**, *42*, 2654.

[21] M. R. Bockstaller, R. A. Mickiewicz, E. L. Thomas, *Adv. Mater.*, **2005**, *17*, 1331.

[22] V. Sankaran, C. C. Cummins, R. R. Schrock, R. E. Cohen, R. J. Silbey, *J.*

Am. Chem. Soc., **1990**, *112*, 6858.

[23] B.-H. Sohn, B.-H. Seo, *Chem. Mater.*, **2001**, *13*, 1752.

[24] B.-H. Sohn, S. I. Yoo, B.-W. Seo, S.-H. Yun, S.-M. Park, *J. Am. Chem. Soc.*, **2001**, *123*, 12734.

[25] Y. Zhao, K. Thorkelsson, A. J. Mastroianni, T. Schilling, J. M. Luther, B. J. Rancatore, K. Matsunaga, H. Jinnai, Y. Wu, D. Poulsen, J. M. J. Frechet, A. P. Alivisatos, T. Xu, *Nat. Mater.*, **2009**, *8*, 979.

[26] M. R. Bockstaller, Y. Lapetnikov, S. Margel, E. L. Thomas, *J. Am. Chem. Soc.*, **2003**, *125*, 5276.

[27] M. K. Gaines, S. D. Smith, J. Samseth, M. R. Bockstaller, R. B. Thompson, K. O. Rasmussen, R. J. SponTak, *Soft Matter*, **2008**, *4*, 1609.

[28] B. J. Kim, J. J. Chiu, G.-R. Yi, D. J. Pine, E. J. Kramer, *Adv. Mater.*, **2005**, *17*, 2618.

[29] H. Kang, F. A. Detcheverry, A. N. Mangham, M. P. Stoykovich, K. C. Daoulas, R. J. Hamers, M. Müller, J. J. de Pablo, P. F. Nealey, *Phys. Rev. Lett.*, **2008**, *100*, 148303.

[30] J. J. Chiu, B. J. Kim, G.-R. Yi, J. Bang, E. J. Kramer, D. J. Pine, *Macromolecules*, **2007**, *40*, 3361.

[31] M. W. Matsen, R. B. Thompson, *Macromolecules*, **2008**, *41*, 1853.

[32] S. Zou, R. Hong, T. Emrick, G. C. Waker, *Langmuir*, **2007**, *23*, 1612.

[33] B. J. Kim, J. Bang, C. J. Hawker, E. J. Kramer, *Macromolecules*, **2006**, *39*, 4108.

[34] S. C. Warren, L. C. Messina, L. S. Slaughter, M. Kamperman, Q. Zhou, S. M. Gruner, F. J. DiSalvo, U. Wiesner, *Science*, **2008**, *320*, 1748.

[35] Y. Lin, V. K. Daga, E. R. Anderson, S. P. Gido, J. J. Watkins, *J. Am. Chem. Soc.*, **2011**, *133*, 6513.

[36] A. Noro, K. Higuchi, Y. Sageshima, Y. Matsushita, *Macromolecules*, **2012**, *45*, 1553.

[37] S. G. Jang, A. Khan, C. J. Hawker, E. J. Kramer, *Macromolecules*, **2012**, *45*, 1553–1561.

[38] K. Thorkelsson, A. J. Mastroianni, P. Ercius, T. Xu, *Nano Lett.*, **2012**, *12*, 498–504.

[39] S. Förster, T. Plantenberg, *Angew. Chem. Int. Ed.*, **2002**, *41*, 689.

[40] Y. Mai, A. Eisenberg, *Chem. Soc. Rev.*, **2012**, *41*, 5969.

[41] F. S. Bates, *Science*, **1991**, *251*, 898.

[42] F. S. Bates, G. H. Fredrickson, *Phys. Today*, **1999**, *52*, 32.

[43] M. J. Fasolka, A. M. Mayes, *Annu. Rev. Mater. Res.*, **2001**, *31*, 323.

[44] R. A. Segalman, *Mater. Sci. Eng. R.*, **2005**, *48*, 191.

[45] P. Mansky, Y. Liu, E. Huang, T. P. Russell, C. J. Hawker, *Science,* **1997**, *275*, 1458.

[46] D. Borah, S. Rasappa, R. Senthamaraikannan, M. T. Shaw, J. D. Holmes, M. A. Morris, *J. Colloid Interface Sci*., **2013**, *393*, 192.

[47] A. Knoll, A. Horvat, K. S. Lyakhova, G. Krausch, G. J. A. Sevink, A. V. Zvelindovsky, R. Magerle, *Phys. Rev. Lett*., **2002**, *89*, 035501.

[48] G. Riess, *Prog. Polym. Sci*., **2003**, *28*, 1107.

[49] M. Antonietti, S. Heinz, M. Schmidt, C. Rosenauer, *Macromolecules,* **1994**, *27*, 3276.

[50] S. Förster, M. Zisenis, E. Wenz, M. Antonietti, *J. Chem. Phys.*, **1996**, *104*, 9956.

[51] L. Zhang, A. Eisenberg, *J. Am. Chem. Soc.*, **1996**, *118*, 3168.

[52] W. A. Braunecker, K. Matyjaszewski, *Prog. Polym. Sci*., **2007**, *32*, 93.

[53] M. Szwarc, *Nature*, **1956**, *176*, 1168.

[54] C. J. Hawker, A. W. Bosman, E. Harth, *Chem. Rev.*, **2001**, *101*, 3661.

[55] K. Matyjaszewski, J. Xia, *Chem. Rev.*, **2001**, *101*, 2921.

[56] G. Moad, E. Rizzardo, S. H. Thang, *Aust. J. Chem.*, **2012**, *65*, 985.

[57] D. J. Keddie, *Chem. Soc. Rev.*, **2014**, *43*, 496.

[58] J.-T. Sun, C.-Y. Hong and C.-Y. Pan, *Soft Matter*, **2012**, *8*, 7753.

[59] A. Das, P. Theato, *Chem. Rev.*, **2016**, *116*, 1434.

[60] H. C. Kolb, M. G. Finn, K. B. Sharpless, *Angew. Chem. Int. Ed.*, **2001**, *40*, 2004.

[61] R. C. Li, R. M. Broyer, H. D. Maynard, *J. Polym. Sci. Part A: Polym. Chem*., **2006**, *44*, 5004.

[62] B. S. Sumerlin, N. V. Tsarevsky, G. Louche, R. Y. Lee, K. Matyjaszewski, *Macromolecules*, **2005**, *38*, 7540.

[63] A. Godwin, M. Hartenstein, A. H. E. Müller, S. Brocchini, *Angew. Chem. Int. Ed.*, **2001**, *40*, 594.

[64] M. Eberhardt, R. Mruk, R. Zentel, P. Theato, *Eur. Polym. J*., **2005**, *41*, 1569.

[65] P. Theato, *J. Polym. Sci. Part A: Polym. Chem.*, **2008**, *46*, 6677.

[66] R. K. Iha, K. L. Wooley, A. M. Nyström, D. J. Burke, M. J. Kade, C. J. Hawker, *Chem. Rev.*, **2009**, *109*, 5620.

[67] K. A. Günay1, P. Theato, H.-A. Klok, *J. Polym. Sci. A : Polym. Chem.*, **2013**, *52*, 1.

[68] M. N. Tahir, F. Natalio, H. A. Therese, A. Yella, N. Metz, M. R. Shah, E. Mugnaioli, R. Berger, P. Theato, H. C. Schröder, W. E. G. Müller, W. Tremel, *Adv. Funct. Mater.*, **2009**, *19*, 285.

[69] M. I. Shukoor, F. Natalio, M. N. Tahir, M. Wiens, M. Tarantola, H. A. Therese, M. Barz, S. Weber, M. Terekhov, H. C. Schröder, W. E. G. Müller, A. Janshoff, P. Theato, R. Zentel, L. M. Schreiber, W. Tremel, *Adv. Funct. Mater.*, **2009**, *19*, 3717.

[70] M. Barz, M. Tarantola, K. Fischer, M. Schmidt, R. Luxenhofer, A. Janshoff, P. Theato, R. Zentel, *Biomacromolecules*, **2008**, *9*, 3114.

[71] F. Jochum, P. Theato, *Chem. Comm.*, **2010**, *46*, 6717.

[72] M. Zorn, M. N. Tahir, B. Bergmann, W. Tremel, C. Grigoriadis, G. Floudas, R. Zentel, *Macromol. Rapid Commun.*, **2010**, *31*, 1101.

[73] J. Kwak, W. K. Bae, M. Zorn, H. Woo, H. Yoon, J. Lim, S. W. Kang, S. Weber, H.-J. Butt, R. Zentel, S. Lee, K. Char, C. Lee, *Adv. Mater.*, **2009**, *21* 5022.

[74] L. zur Borg, D. Lee, J. Lim, W. K. Bae, M. Park, S. Lee, C. Lee, K. Char, R. Zentel, *J Mater. Chem. C*, **2013**, *1*, 1722.

Chapter II.

Spatial Arrangement of Quantum Dots Directed by Block Copolymer Lamellar Nanostructures in Composite Films

2-1. Introduction

Quantum dots (QDs) are solution-processed nanoscale crystals of semiconducting materials. The unique size-dependent optical properties of QDs have motivated increasingly active research aimed at applying them in the next generation of optoelectronic and biomedical technologies.[1-5] To apply QDs to devices fabrication, they should be processable into technologically applicable form such as films or spherical bids.[6] One of the widely used way to enable that is hybridization with polymer matrix materials.[7-10] Polymers can offer an easy processability, a transparency in the visible range and an excellent mechanical and chemical stability.[11-12]

Among these polymers, diblock copolymers are considered as desirable matrix materials because they spontaneously form nanostructures such as spheres, cylinders, and lamellae, which can be used to incorporate QDs, via self-assembly.[13-15] The arrangement of incorporated QDs thus can be manipulated by controlling the nanostructures of diblock copolymers. Nanoparticles, including QDs, however, tend to aggregate each other due to their inherently large surface-to-volume ratios. To apply QDs to optical device fabrication without loss of the optical properties, controlled dispersion is indispensable to avoid undesirable coupling between themselves. To overcome this problem, the surface of nanoparticles and/or polymeric matrices need to be modified to have

preferential enthalpic interaction. [15,16]

In this chapter, we demonstrate spatial arrangement of QDs directed by lamellar nanostructure of functional block copolymers in composite films. As a polymer matrix which can direct the arrangement of QDs, we synthesize a diblock copolymer having a reactive block then thiol functionalities which can interact with QDs are introduced along the reactive block by postpoymerization modification. Thin films of block copolymer with QDs are fabricated by spin-coating with various thickness. Perpendicularly- and parallelly-oriented lamellar nanostructures are developed by solvent annealing and QDs were selectively arranged. And free-standing film with QD-arranged lamellar nanostructure with random orientation is also fabricated by solvent-casting. Absorbance and photo luminescent properties of QDs are preserved in films.

2-2. Experimental Section

Materials

All chemicals were commercially available and were used as received unless noted. 2,2'-Azoisobutyronitrile (AIBN) was recrystallized from ethanol. Benzene was distilled under nitrogen. Pentafluorophenylmethacrylate (PFPMA) and cumyldithiobenzoate, a chain transfer agent (CTA), were synthesized according to the literatures. Methylmethacrylate (MMA) and PFPMA were distilled under reduced pressure.

Synthesis of Block Copolymers

5.0 g (50 mmol) of MMA, 45 mg (0.167 mmol) of cumyldithiobenzoate, and 3.4 mg (0.05 mmol) of AIBN were added to 3 ml of distilled benzene, and then air was exchanged with argon by three freeze-thaw cycles. Polymerization of methylmethacrylate (MMA) was carried out at 75 °C for 21 hr. Poly(methylmethacrylate) (PMMA) polymers were purified by precipitating them into cold ethanol. Two more precipitations were performed from their THF solutions. After drying at 30 ℃ for 4 hr in vacuum, 3.5 g (70%) of PMMA was obtained in pink powders. The number average molecular weight is 79,000 g mol-1 and the polydispersity index is 1.09. Then, 2.0 g (16.7 mmol) of PMMA, which

can act as macro-CTA,[17] was dissolved in 5 mL of benzene. 0.0685 mg (0.0042 mmol) of AIBN and 3.5 g (13.8 mmol) of pentafluorophenylmethacrylate (PFPMA), a monomer for the second block, were added. The whole mixture was heated to 70 ℃ under argon and polymerization was carried out for 48 hr. Block copolymers were purified as before, yielding 4.0 g (57%) of Poly(methylmethacrylate)-*block*-poly(pentafluorophenylmethacrylate) (PMMA-PPFPMA) in pale pink powders.[18] PMMA-PPFPMA copolymers show that the weight ratio between two blocks is 1 : 1 (Figure 2-2a NMR) and the polydispersity index is 1.29.

Thiol Functionalization of PMMA-PPFPMA Block Copolymers

For synthesis of thiol-functionalized PMMA-P(PFPMA-SH) copolymers, 200 mg (1.26 μmol) of PMMA-PPFPMA was dissolved in 10 mL of THF, and then 1.6 mg (20 μmol) of cysteamine was added. The mixture was stirred for 24 h at 50 ℃ under nitrogen. Functionalized copolymers were precipitated into cold methanol and dried under vacuum. 190 mg of colorless powders was obtained.

Preparation of Films

A thin film was spin-coated on a silicon wafer or a quartz plate (2000 rpm, 60 s) from a solution which contains PMMA-PPFPMA alone, a blend of PMMA-P(PFPMA-SH)/QDs. All spin-coated films were annealed in saturated THF vapor for 24 h. For a solution containing QDs, PMMA-P(PFPMA-SH) and QDs were mixed in toluene, sonicated for 5 min, precipitated in hexane, and dried in powder form. The mixed powder of PMMA-P(PFPMA-SH) and QDs was then dissolved in toluene again. A free-standing bulk film of PMMA-PPFPMA or a blend of PMMA-P(PFPMA-SH)/QDs was also casted slowly from its toluene solution (5 wt%) at room temperature for several days and then was dried at a reduced pressure.

Characterization

NMR spectra were obtained on a Varian NMR System (500 MHz). Gel permeation chromatography (GPC) was carried out on a Waters system (1515 pump, 2414 refractive index detector) with a Shodex GPC LF-804 column. Transmission electron microscopy (TEM) analysis was performed on a Hitachi 7600 operating at 100 kV. For cross-sectional TEM, bulk and thin films were embedded in epoxy with carbon coating on both sides of the film and were cured

at 60 °C for 12 h. Thin sections (~80 nm thick) were obtained using an RMC MTX ultramicrotome with a diamond knife. UV-Vis absorption spectra were recorded on a Scinco S-3100 spectrophotometer. Photoluminescence measurements were performed with an Acton spectra pro 2300i.

2-3. Results and Discussion

QDs we used in this chapter are comprised comprised of core-shell CdSe@ZnS capped with oleic acid,[19] which are shown in the TEM image of Figure 2-1a. The shape of these QDs is not completely spherical due to the presence of a thick ZnS shell[4] that made a relatively large diameter of 8.7 nm (±0.6 nm) but was necessary for stable green emission at 501 nm (Figure 2-1b).

To prepare a block copolymer matrix which is capable to arrange QDs in the self-assembled nanostructure, we first synthesized a block copolymer having a reactive block capable of anchoring various functional groups covalently in a feasible and quantitative manner then thiol groups were introduced onto the side chain of reactive block by post-polymerization modification. For the reactive block, we selected poly(pentafluorophenylmethacrylate) (PPFPMA) with an activated ester which can form an amide bond with a reaction with various primary amines.[20] Poly(methylmethacrylate) (PMMA) was chosen for the

other block, which can be easily synthesized by RAFT and be optically clear. As shown in Figure 2-1(a), we synthesized PPFPMA-PMMA block copolymers by RAFT polymerization. PMMA, which was synthesized with cumyldithiobenzoate as a chain transfer agent (CTA), was used as a macro-CTA to polymerize the PPFPMA block.

We investigated the nanostructure of PMMA(79)–PPFPMA(79) copolymers in a thin film with different thickness on a substrate such as silicon wafer or quartz to applicate as a matrix for an optical devices. The number in parentheses is the number average molecular weight in kg/mol. A thin film (~76 nm thick) was fabricated by spin-coating of 1.5 wt% copolymer solution and then annealed by THF solvent vapor. In the TEM image of Figure 2-2(a) shows fingerprint pattern consisting of bright PMMA lamellae and dark PPFPMA lamellae which are perpendicular to the plane of the film. The average lamellar period is 72 nm, which is similar to that of a thermally annealed bulk film.

On the other hand, a thicker film (~140 nm thick) was fabricated by spin-coating of 3 wt% copolymer solution and then the lamellar nanostructure was induced by solvent annealing. Figure 2-2(c) is a cross-sectional TEM image of a thin film of PMMA–PPFPMA copolymers. Irregular black parts on both sides of the film are carbon layers that were coated before epoxy embedding during the sampling process for TEM. [21] Between these carbon coatings, we can find

alternate layers of bright PMMA lamellae and dark PPFPMA lamellae, which are parallel to the plane of the film. The parallel lamellae in a thin film of block copolymers can be generally observed due to the preference of each block to the interface of the substrate or the air. [22] In this case, we presume that the polar PMMA block favors the native oxide layer of the silicon wafer and the fl uorinated PPFPMA block prefers the air interface. The average lamellar period is 28 nm, much smaller than that of a thermally annealed bulk film due to rapid solven removal process in the end of solvent vapor annealing.[23,24]

To give a compatibility with QDs along PPFPMA block, a small portion of activated esters in the PPFPMA block was reacted with cysteamine which contain thiol functional groups as shown in Figure 2-1(b). Thus, PMMA-P(PFPMA-SH) copolymers have thiol functional groups, which can allow QDs to be incorporated into the lamellar structure of the PPFPMA block.

With the thiol functionality in PMMA-P(PFPMA-SH) as a matrix, we fabricated thin films having lamellar nanostructure which contains QDs selectively in PPFPMA domain. QDs were blended with thiol-functionalized PMMA-P(PFPMA-SH) in toluene, followed by stirring at 50 ^{o}C for 2 h. Thin films were fabricated by spin coating, and then the lamellar nanostructure was induced by solvent annealing.

Perpendicularly oriented nanostructure of a thin film (~78 nm thick) of block

copolymer with QDs is shown in Figure 2-3(b). We can find a fingerprint pattern consisting of bright PMMA lamellae and dark PPFPMA lamellae as like the previous image of Figure 2-3(a). However QDs are additionally found as black dots which are localized in the PPFPMA lamellae. The selective incorporation of QDs into PPFPMA lamellae can be attributed to thiol-functionalized PMMA-P(PFPMA-SH) which would not be phase-separated from PMMA-PPFPMA because of the small amount of thiol groups in PMMA-P(PFPMA-SH).

In a thin film of block copolymers with QDs with ~120 nm thickness, a lamellar structure parallel to the plane of substrate was developed. A cross-sectional TEM image of a thin film is shown in Figure 2-3(d). We can find carbon layers on both sides of the film and the alternate layers of bright PMMA lamellae and dark PPFPMA lamellae parallel to the plane of the film as like the previous image of Figure 2-3(c) and QDs are also found additionally as black dots which are localized in the dark PPFPMA lamellae.

The fluorescent properties of QDs in these thin films were examined. As shown in figure 2-4(a), PL spectrum of films are almost identical to that of pristine QDs (Figure 2-1(b)) and the PL intensities of films were proportional to their thickness(Figure 2-4(b)), implying that QDs are well dispersed without aggregation.

We also fabricated free-standing film of PMMA-P(PFPMA-SH) with QDs. A

film was prepared with several micrometers thickness by slow-casting of 1.0 g of 5 wt% toluene solution of PMMA(55)-P(PFPMA-SH)(77) with QDs in a Teflon-coated boat. As shown in the cross-sectional TEM image of Figure 2-5(a), lamellar nanostructure was well-developed. The average lamellar period is 32 nm. The TEM image of Figure 2-5(b) is a free-standing film of PMMA(55)-P(PFPMA-SH)(77) with QDs. Lamellar nanostructure can be clearly observed and QDs are also found selectively in dark PPFPMA lamellae. PL spectrum and UV/vis absorbance of film are almost identical to that of pristine QDs, implying that QDs in free-standing film are well dispersed without aggregation.

2-4. Conclusion

In summary, we demonstrated spatial arrangement of QDs directed by lamellar nanostructure of thiol-functionalized PMMA-P(PFPMA-SH) in thin films and free standing film. As a polymer matrix which can direct the arrangement of QDs, we synthesized PMMA-PPFPMA diblock copolymer which have a reactive ester then thiol functionalities which can interact with QDs were introduced along the PPFPMA block by postpolymerization modification. Thin films of block copolymer with QDs are fabricated by spin-coating with various thickness. Lamellar nanostructures with perpendicular and parallel orientation were developed by solvent annealing and QDs were arranged along PPFPMA lamellae. And free-standing film with QD-arranged lamellar nanostructure with random orientation was also fabricated by solvent-casting. Absorbance and photo luminescent properties of QDs are preserved in films.

2-5. References

[1] C. B. Murray, D. J. Norris, M. G. Bawendi, *J. Am. Chem. Soc.*, **1993**, *115*, 8706.

[2] M. A. Hines, P. Guyot-Sionnest, *J. Phys. Chem. B,* **1996**, *100*, 468.

[3] Y. Shirasaki, G. J. Supran, M. G. Bawendi, V. Bulovic, *Nat. Photonics*, **2013**, *7*, 13.

[4] B. O. Dabbousi, J. R. Viejo, F. V. Mikulec, J. R. Heine, H. Mattoussi, R. Ober, K. F. Jensen, M. G. Bawendi, *J. Phys. Chem. B,* **1997**, *101*, 9463.

[5] C. A. Leatherdale, W. K. Woo, F. V. Mikulec, M. G. Bawendi, *J. Phys. Chem. B,* **2002**, *106*, 7619.

[6] M. Zorn, W. K. Bae, J. Kwak, H. Lee, C. Lee, R. Zentel, K. Char, *ACS Nano*, **2009**, *3*, 1063.

[7] J. Lee, V. C. Sundar, J. R. Heine, M. G. Bawendi, K. F. Jensen, *Adv. Mater*., **2000**, *12*, 1102.

[8] H. Zhang, Z. Cui, Y. Wang, K. Zhang, X. Ji, C. Lü, B. Yang, M. Gao, *Adv. Mater*., **2003**, *15*, 777.

[9] H. Du, G. Q. Xu, W. S. Chin, *Chem. Mater*., **2002,** *14*, 4473.

[10] H. Song, S. Lee, *Nanotechnology,* **2007**, *18*, 055402.

[11] L. L. Beecroft, C. K. Ober, *Chem. Mater.*, **1997,** *9*, 1302.

[12] E. Glogowski, R. Tangirala, T. P. Russell, T. Emrick, *J. Pol. Sci. A Pol. Chem*., **2006**, *4*, 5076.

[13] Y. Mai, A. Eisenberg, *Chem. Soc. Rev.,* **2012**, *41*, 5969.

[14] J. Kao, K. Thorkelsson, P. Bai, B. J. Rancatore, T. Xu, *Chem. Soc. Rev.*, **2013**, *42*, 2654.

[15] B. Sarkar, P. Alexandridis, *Prog. Polym. Sci.*, **2015**, *40*, 33.

[16] L. Yao, Y. Lin, J. J. Watkins, *Macromolecules*, **2014**, *47*, 1844.

[17] Y. K. Chong, T. P. T. Le, G. Moad, E. Rizzardo, S. H. Thang, *Macromolecules,* **1999**, *32*, 2071.

[18] M. Eberhardt, P. Theato, *Macromol. Rapid Commun.*, **2005**, *26*, 1488.

[19] W. K. Bae, K. Char, H. Hur and S. Lee, *Chem. Mater.*, **2008**, *20*, 531.

[20] A. Das, P. Theato, *Chem. Rev.*, **2016**, *116*, 1434.

[21] S. Kim, J. Lee, S.-M. Jeon, H. H. Lee, K. Char, B. H. Sohn, *Macromolecules,* **2008**, *41*, 3401.

[22] H.-C. Kim, S.-M. Park, W. D. Hinsberg, *Chem. Rev.*, **2010**, *110*, 146.

[23] K. Fukunaga, T. Hashimoto, H. Elbs, G. Krausch, *Macromolecules*, **2002**, *35*, 4406.

[24] J. Peng, D. H. Kim, W. Knoll, Y. Xuan, B. Li, Y. Han, *J. Chem. Phys.*, **2006**, *125*, 064702.

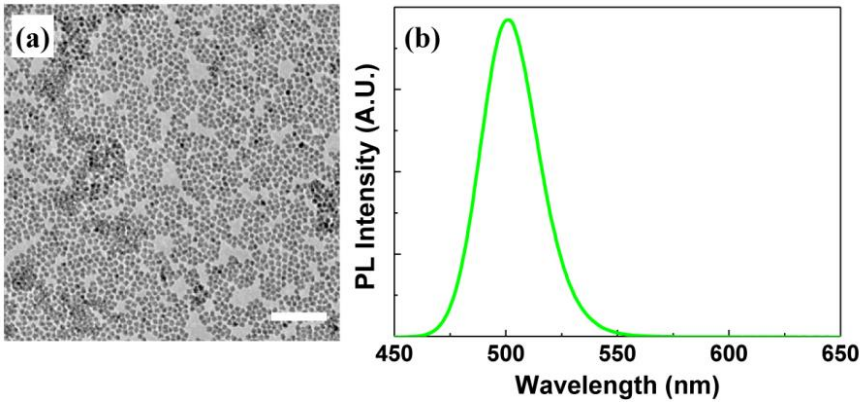

Figure 2-1. CdSe@ZnS QDs: (a) TEM image; (b) PL spectrum. The scale bar in the image is 100 nm. The excitation wavelength for the PL was 360 nm.

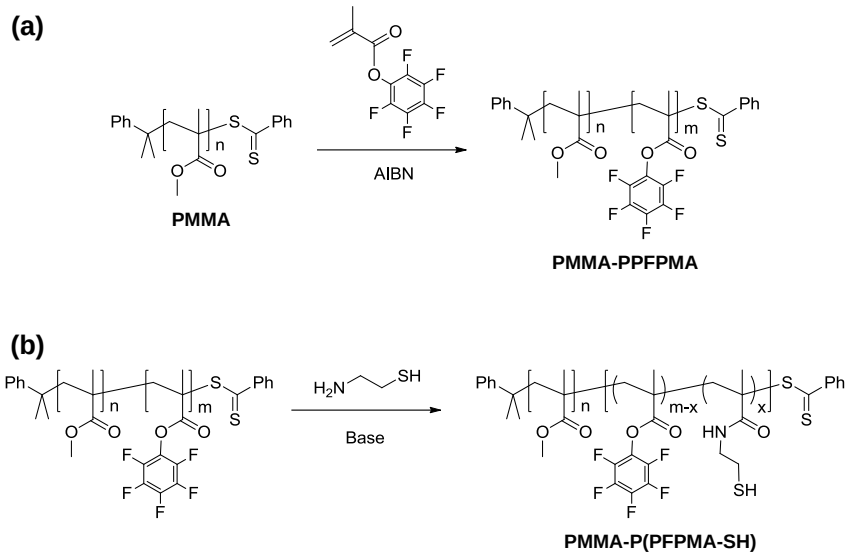

Figure 2-2. Synthetic schemes: (a) RAFT Polymerization of PMMA-PPFPMA; (b)Thiol-functionalization of PMMA-PPFPMA

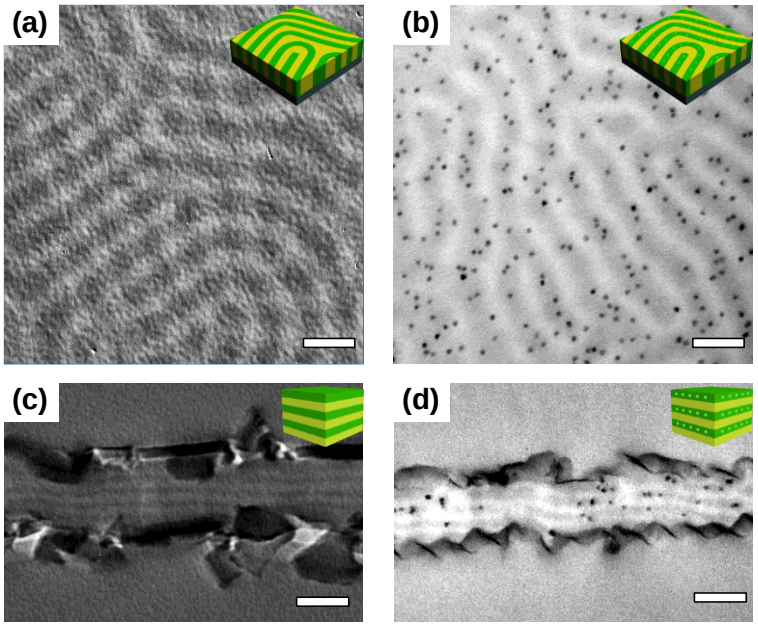

Figure 2-3. TEM images of thin films with perpendicularly oriented lamellar nanostructures: (a) PMMA-PPFPMA; (b) mixture of PMMA-P(PFPMA-SH) and QDs. Cross-sectional TEM images of thin film with parallel oriented lamellar nanostructures: (c) PMMA-PPFPMA; (d) mixture of PMMA-P(PFPMA-SH) and QDs, The scale bars in the images are 100 nm.

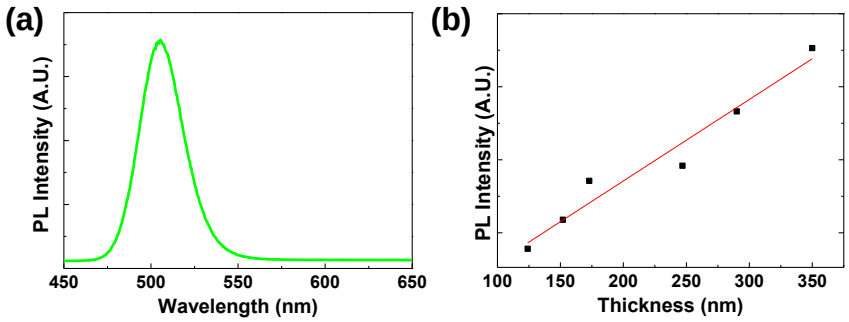

Figure 2-4. PL Spectrum of thin films of PMMA-P(PFPMA-SH) with QDs. The excitation wavelength for the PL was 360 nm.

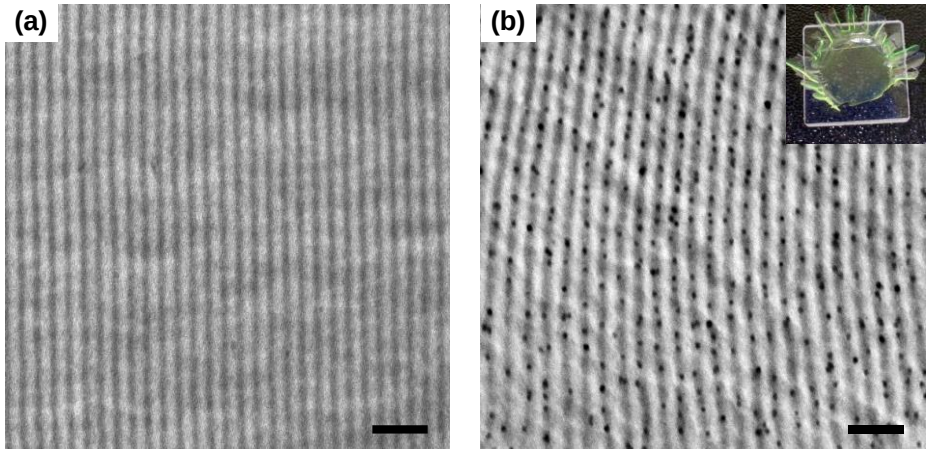

Figure 2-5. Cross-sectional TEM images of casted films: (c) PMMA-PPFPMA; (d) mixture of PMMA-P(PFPMA-SH) and QDs, The scale bars in the images are 100 nm.

Chapter 3.

Simultaneous Incorporation of Dual Fluorophores into Nanostructures of Functional Block Copolymers

3-1. Introduction

In recent years, many efforts have been focused on “bottom-up” approaches to fabricate functional nanostructures.[1-12] Block copolymers have been considered one of the promising functional nanomaterials for device applications, because their self-assembled structure enables to create functionalized nanostructures by incorporating the functional block which has conductive,[4,5] fluorescent,[6] stimulus-responsive,[7] cross-linkable,[8] degradable,[9] metal-coordinative,[10] or liquid crystalline[11] characteristics. More examples can be found in the recent review article describing block copolymer-based nanomaterials.[12]

In the previous chapter, we focused on the arrangement of nanoparticles directed by block copolymer nanostructures. Based on these structures, other functionalities can be combined by simultaneous incorporation into arranged nanostructures to introduce properties complementary to those of nanoparticles.[2,13] From these simultaneous incorporation, unique physical and chemical properties can be induced by conjunction between them. Especially organic small molecules which have optical, electrical, and magnetic properties, possess numerous advantages to provide tunable functionalities for nanomaterials.[2]

In chapter 3, we demonstrate simultaneous arrangement of two fluorophores

directed by nanostructures of block copolymers. For this purpose, we used a strategy of blending of thiol-functionalized block copolymer which is used in chapter 2 and organic fluorophore-anchored block copolymer which has the same basic chemical structure for each block but differ in small amounts of functional moieties in one of the blocks so that they can come into the same nanostructure. Organic fluorophores are also introduced along the reactive block by post-polymerization modification demonstrated in chapter 1, and lamellar nanostructures was also confirmed. With a blending strategy of two functionalized block copolymers, quantum dots (QDs) and organic fluorophores are simultaneously arranged into lamellar nanostructures of block copolymers. We observed the fluorescence resonance energy transfer (FRET) between QDs and organic fluorophores which were concurrently confined in the nanoscale domains.

3-2. Experimental Section

Materials

All chemicals were commercially available and were used as received. Poly(methylmethacrylate)-*block*-poly(pentafluorophenylmethacrylate) (PMMA-PPFPMA, The number average molecular weight: PMMA ~79,000 g/mol and PPFPMA ~79,000 g/mol, PDI ~1.09) block copolymers were used which was synthesized in previous chapter.

Functionalization of PMMA-PPFPMA Block Copolymers

Thiol-functionalized PMMA-P(PFPMA-SH) copolymers were used which was synthesized in previous chapter. For synthesis of fluorophore-functionalized PMMA-P(PFPMA-TAMRA) copolymers, 200 mg (1.26 μmol) of PMMA-PPFPMA was dissolved in 10 mL of THF, and then 5 mg (8 μmol) of tetramethylrhodamine-5-carboxamide (5-TAMRA) cadaverine was added. Then, the same procedure as explained for thiol-functionalized copolymers was followed again. 160 mg of TAMRA-functionalized copolymers was obtained in red powders.

Preparation of Films

A thin film (~120 nm thick) was spin-coated on a silicon wafer or a quartz plate (2000 rpm, 60 s) from a solution which contains PMMA-PPFPMA alone, a blend of PMMA-PPFPMA/PMMA-P(PFPMA-SH)/QDs, a blend of PMMA-PPFPMA/PMMA-P(PFPMA-TAMRA), or a blend of PMMA-P(PFPMA-SH)/QDs/PMMA-P(FPMA-TAMRA). All spin-coated films were annealed in saturated THF vapor for 24 h. For a solution containing QDs, PMMA-P(PFPMA-SH) and QDs were mixed in toluene, sonicated for 5 min, precipitated in hexane, and dried in powder form. The mixed powder of PMMA-P(PFPMA-SH) and QDs was then dissolved in toluene again with PMMA-PPFPMA or PMMA-P(FPMA-TAMRA). A bulk film of PMMA-PPFPMA was also casted slowly from its toluene solution (5 wt%) at room temperature for several days and then was thermally annealed at 210 ℃ for 36 h in vacuum.

Characterization

NMR spectra were obtained on a Varian NMR System (500 MHz). Transmission electron microscopy (TEM) analysis was performed on a Hitachi 7600 operating at 100 kV. For cross-sectional TEM, bulk and thin films were embedded in epoxy with carbon coating on both sides of the film and were cured at 60 °C for 12 h. Thin sections (~80 nm thick) were obtained using an RMC MTX ultramicrotome with a diamond knife. UV-Vis absorption spectra were

recorded on a Scinco S-3100 spectrophotometer. Photoluminescence measurements were performed with an Acton spectra pro 2300i.

3-3. Results and Discussion

In the previous chapter, we functionalized PMMA-PPFPMA with a small amount of thiol functionalities. To prepare fluorophore-functionalized block copolymer which has which has the same basic chemical structure that enable to make same nanostructures without macro-phase separation after mixing, we synthesized PMMA-P(PFPMA-TAMRA) copolymers by linking 2 mol% TAMRA, an organic fluorescent dye, to the PPFPMA block as shown in Figure 3-1. From the NMR date of Figure 3-2, we confirmed TAMRA were successfully attached covalently along the PPFPMA block. And we examined fluorescence of PMMA-P(PFPMA-TAMRA) in toluene solution. The maximum emission is located at 572 nm, which is almost identical to that of pristine TAMRA.

In the previous chapter, we investigated the nanostructure of PMMA-PPFPMA copolymers in a thin film on a glass substrate. In the thin film (~140 nm thick) of the copolymer, lamellar structure parallel to the plane of the film was observed and the average lamellar period was 28 nm. In a similar manner we fabricated a thin film (~140 nm thick) of PMMA-P(PFPMA-TAMRA). A cross-

sectional TEM image of a thin film of TAMRA-functionalized block copolymers is shown in Figure 3-2. We can find carbon layers on both sides of the film and the alternate layers of bright PMMA lamellae and dark PPFPMA lamellae parallel to the plane of the film as like the image of pristine PMMA-PPFPMA thin film. Organic TAMRA dyes are indistinguishable in TEM so that we cannot expect any difference in a TEM image, compared to that without the TAMRA functionality. In contrast to a thin film of pristine PMMA-PPFPMA, however, this thin film functionalized with TAMRA shows a red emission centered at 568 nm as shown in PL spectrum of Figure 3-2. This PL result implies that PPFPMA lamellae can be functionalized with TAMRA as shown in a schematic illustration of Figure 3-2.

We induced dual functionalization of lamellar nanostructures of block copolymers by simultaneous incorporation of QDs and fluorescent dyes, which were independently introduced to the lamellar nanostructure in the previous cases. Similarly as before, we fabricated a thin film (~120 nm thick) consisting of QDs, thiol-functionalized PMMA-P(PFPMA-SH), and TAMRA-functionalized PMMA-P(PFPMA-TAMRA). Then, we investigated nanostructures and fluorescent characteristics of the thin film.

Particularly for comparison of fluorescent properties of this dual functionalized film with those of the film only with QDs or only with TAMRA, the equal amount of QDs and TAMRA dyes in each film should be guaranteed. A

relative amount of fluorophores can be generally found by UV-Vis absorption spectra.[14] However, a thin film has a very small amount of fluorophores, which makes it difficult to obtain a reasonable absorption spectrum. Since we spin-coated a thin film with an almost identical thickness from each solution in every case, we measured an UV-Vis absorption spectrum of the solution used for spin coating to confirm an equal amount of fluorophores in each film.

Figure 3-4 shows UV-Vis spectra of the solutions used for spin coating. In the spectrum only with QDs (green dashed line), a broad absorption below 510 nm can be observed. We can find the same broad absorption below 510 nm again in the spectrum with QDs and TAMRA (pink solid line), implying the equal amount of QDs in both cases. In the case of TAMRA only (red dashed line), an absorption peak between 450 and 600 nm with the maximum at 552 nm can be found, which can be again observed in the spectrum with QDs and TAMRA (pink solid line). Thus, we can also confirm the equal amount of TAMRA in both cases. Since a film with the same thickness was spin-coated from each of these solutions, we can compare PL spectra of thin films, assuming the equal amount of fluorophores in each film. The fluorescent results are shown in Figure 3-5.

Figure 3-5 shows a cross-sectional TEM image of a thin film consisting of QDs, thiol-functionalized PMMA-P(PFPMA-SH), and TAMRA-functionalized PMMA-P(PFPMA-TAMRA). We can find the alternate layers of bright PMMA lamellae and dark PPFPMA lamellae between the carbon layers on

both side of the film. We can also find the QDs localized in the PPFPMA lamellae. Although organic TAMRA dyes are indistinguishable in TEM, we can expect that TAMRA would exist in the PPFPMA lamellae because 2 mol% TAMRA in P(PFPMA-TAMRA) would not cause phase-separation from PPFPMA and P(PFPMA-SH).

PL spectra of the films only with QDs (green dashed line) and only with TAMRA (red dashed line) are given again in Figure 3-5. The weak emission of TAMRA can be mainly ascribed to the weak absorption at the excitation wavelength (360 nm) as shown in the UV-Vis spectrum (red dashed line in Figure 3-4). In contrast, a thin film with both QDs and TAMRA (pink solid line) exhibits a decreased emission of QDs at 502 nm and a greatly enhanced emission of TAMRA at 568 nm. This PL spectrum can be explained by the fluorescence resonance energy transfer (FRET) from quantum dot donors to TAMRA acceptors,[15] both of which are located in the same PPFPMA lamellar nanostructure.

For a quantitative explanation of emission spectra of quantum dots and TAMRA, we calculated the average distance between QDs and TAMRA. The Förster radius of QDs and TAMRA was calculated based on following equation (3-1),[16]

$$R_0 = \frac{9000(\ln 10)\kappa^2 Q_D J}{128\pi^5 n^4 N_{AV}} \quad (3\text{-}1)$$

where Q_D is the fluorescence quantum yield of the donor, κ^2 is the orientation factor, n is the index of refraction of the medium, and J is the overlap integral, which represents the degree of overlap between the donor emission spectrum and the acceptor absorption spectrum.

For $Q_{D,}$ the fluorescence quantum yield of quantum dots isolated in the film at room temperature was approximately calculated as 0.84. The orientation of transition dipoles of the donor and the acceptor is assumed to be random, and a value of 2/3 is assumed to κ^2. The refractive index was assumed as 1.49 which is the one of PMMA. A value for the Förster radius (R_0) was calculated as 4.5 nm.

The FRET efficiency (E) is calculated from $E = 1 - F_{DA}/F_D$, where F_{DA} and F_D are the integrated fluorescence intensity of the quantum dot donor with and without the TAMRA acceptor, respectively. The estimated FRET efficiency (E) is 0.46. Then, the distance (r) between the quantum dot donor and the TAMRA acceptor is calculated from $E = R_0^6/(R_0^6 + r^6)$. Thus, the estimated distance (r) is 4.6 nm.

Since FRET is inversely proportional to the 6th power of the distance between the donor and the acceptor, it has played an important role in the determination of nanometer-scale distances in various systems with high accuracy,[17] which makes FRET called a spectroscopic ruler.[18] Thus, if QDs and TAMRA were separated into different lamellae, there would not be the FRET between them and would be a PL spectrum of the simple addition of two spectra

of QDs (green dashed line) and TAMRA (red dashed line). Therefore, the energy transfer from QDs to TAMRA implies the dual functionalization of the PPFPMA lamellar nanostructures with QDs and TAMRA. We showed the dual functionalization of the lamellae in a schematic illustration of Figure 8.

3-4. Conclusion

In conclusion, we demonstrated simultaneous arrangement of QDs and organic fluorophores directed by nanostructures of block copolymers by blending two block copolymers which have different functional groups. Organic fluorophores, TAMRA, were introduced along the PPFPMA block by post-polymerization modification, and lamellar nanostructures was also confirmed. With a blending strategy of two functionalized block copolymers, QDs and organic fluorophores are simultaneously arranged into lamellar nanostructures of block copolymers. We also observed the enhanced fluorescence of TAMRA by the FRET from the quantum dot donor to the TAMRA acceptor because of their nanoscale confinement. The simultaneous incorporation of two different functionalities can allow expecting a unique property induced by a coupling effect between two functionalities such as FRET and plasmonic coupling based on the nanoscale localization.

3-5. References

[1] A. Haryono, W. H. Binder, *Small*, **2006**, *2*, 600.

[2] J. Kao, K. Thorkelsson, P. Bai, B. J. Rancatore, T. Xu, *Chem. Soc. Rev.*, **2013**, *42*, 2654.

[3] B.-H. Sohn, S. I. Yoo, B.-W. Seo, S.-H. Yun, S.-M. Park, *J. Am. Chem. Soc.*, **2001**, *123*, 12734.

[4] M. Sommer, S. M. Lindner, M. Thelakkat, *Adv. Funct. Mater.*, **2007**, *17*, 1493.

[5] H. C. Moon, D. Bae, J. K. Kim, *Macromolecules*, **2012**, *45*, 5201.

[6] J. You, J. A. Yoon, J. Kim, C.-F. Huang, K. Matyjaszewski, E. Kim, *Chem. Mater*., **2010**, *22*, 4426.

[7] M. A. C. Stuart, W. T. S. Huck, J. Genzer, M. Müller, C. Ober, M Stamm, G. B. Sukhorukov, I, Szleifer, V. V. Tsukruk, M. Urban, F. Winnik, S. Zauscher, I. Luzinov, S. Minko, *Nat. Mater.*, **2010**, *9*, 101.

[8] E. Kim, C. Shin, H. Ahn, D. Y. Ryu, J. Bang, C. J. Hawker, T. P. Russell, *Soft Matter*, **2008**, *4*, 475.

[9] R.-M. Ho, C.-K. Chen, Y.-W Chiang, B.-T. Ko, C.-C. Lin, *Adv. Mater*., **2006**, *18*, 2355.

[10] Y. N. C. Chan, R. R. Schrock and R. E. Cohen, *Chem. Mater.*, **1992**, *4*, 24–27.

[11] M. Gopinadhan, P. W. Majewski, E. S. Beach, C. O. Osuji, *ACS Macro Lett*., **2012**, *1*, 184.

[12] S. I. Yoo, J.-H. Kwon, B. H. Sohn, *J. Mater. Chem.*, **2001**, *17*, 2969.

[13] M. Zorn, W. K. Bae, J. Kwak, H. Lee, C. Lee, R. Zentel, K. Char, *ACS Nano*, **2009**, *3*, 1063.

[14] J. R. Lakowicz, *Principles of Fluorescence Spectroscopy*; Plenum: New York, 1983.

[15] A. R. Clapp, I. L. Medintz, J. M. Mauro, B. R. Fisher, M. G. Bawendi, H. Mattoussi, *J. Am. Chem. Soc.*, **2004**, *126*, 301.

[16] J. R. Lakowicz, Principles of Fluorescence Spectroscopy; Plenum: New York, 1983.

[17] F. Morgner, D. Geiβler, S. Stufler, N. G. Butlin, H.–G. Löhmannsröben, N. Hildebrandt, *Angew. Chemie. Int. Ed*., **2010**, *49*, 7570.

[18] L. Stryer, *Annu. Rev. Biochem*., **1978**, *47*, 819.

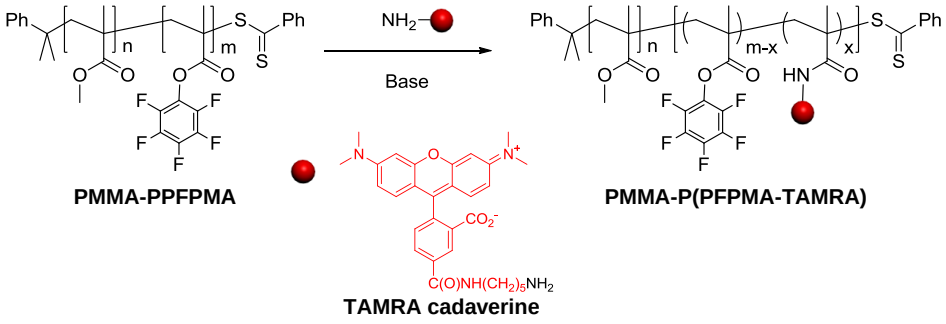

Figure 3-1. Synthetic scheme: fluorophore functionalization of PMMA-PPFPMA

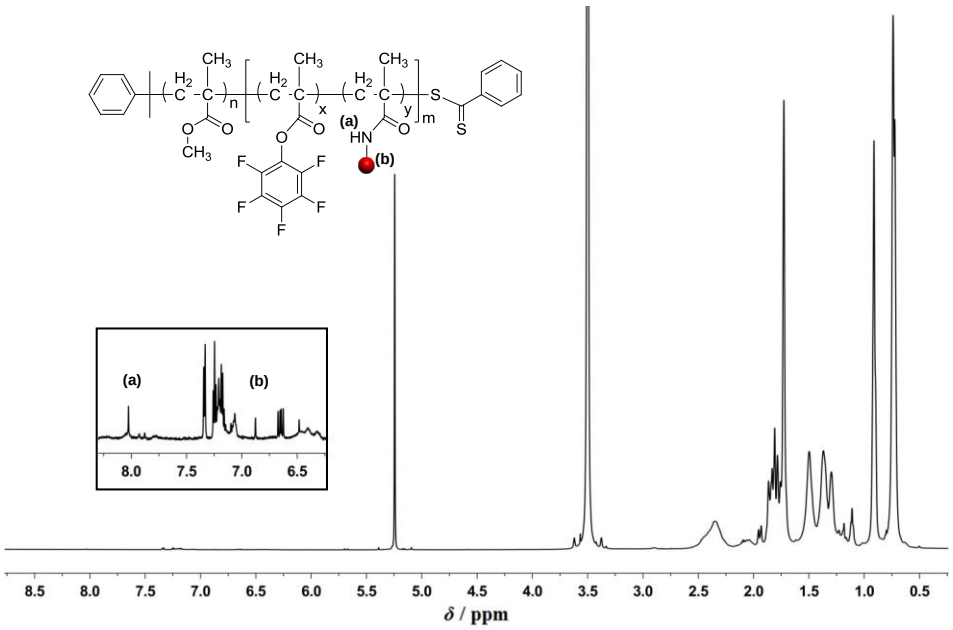

Figure 3-2. ^{1}H NMR of PMMA-P(PFPMA-SH) in CD_2Cl_2

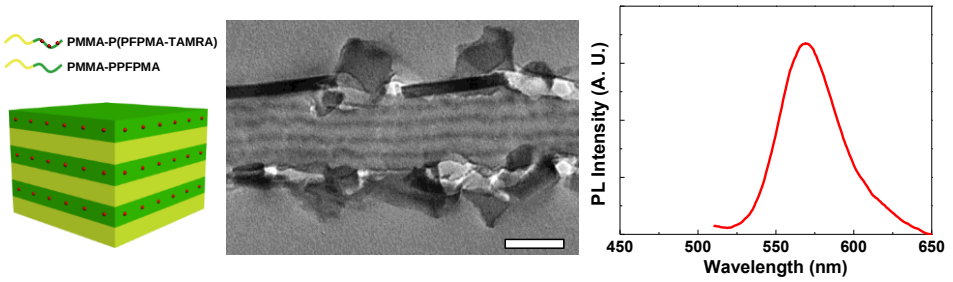

Figure 3-3. Schematic illustration of lamellar nanostructures in a thin film of PMMA-P(PFPMA-TAMRA) (left), cross-sectional TEM image (center) and PL spectrum of the film (right). The excitation wavelength was 360 nm.

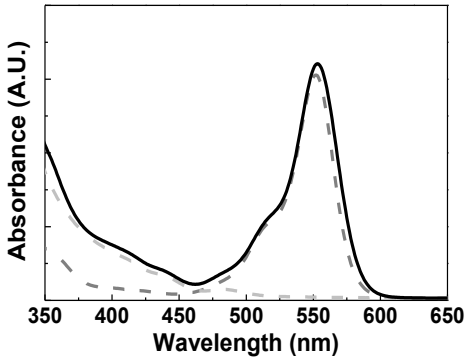

Figure 3-4. UV-Vis spectra of the solutions used for spin coating of thin films of block copolymers: only with QDs (light grey dashed line); only with TAMRA (dark grey dashed line); with both QDs and TAMRA (black solid line).

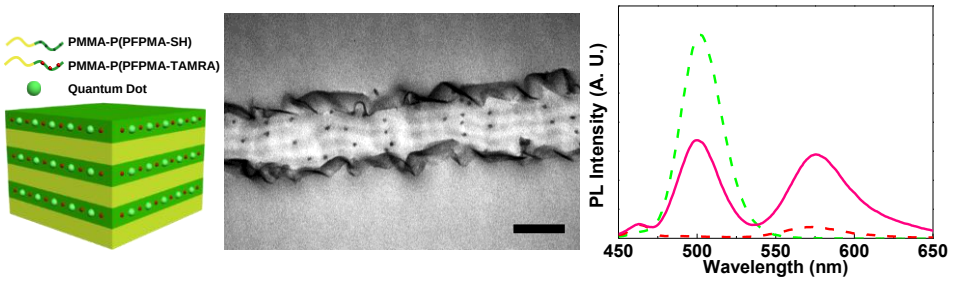

Figure 3-5. Schematic illustration (left), cross-sectional TEM image (center), and PL spectrum (right) of a thin film consisting of QDs, PMMA-P(PFPMA-SH), and PMMA-P(PFPMA-TAMRA). The scale bar in the image is 100 nm. The excitation wavelength for the PL was 360 nm. PL spectra of thin films only with QDs (green dashed line) and only with TAMRA (red dashed line) are displayed together.

Chapter 4.

Fluorescent Supracolloidal Polymer Chains of Quantum Dots Encapsulated by Diblock Copolymer Micelle

4-1. Introduction

Advances in the synthetic methods for uniform spherical nanoparticles of metals, oxides, and semiconductors have enabled the effective creation of their superlattices as well as colloidal crystals.[1-7] For example, uniform CdSe quantum dots (QDs), which show size-dependent and well-defined fluorescence,[3] assembled into a superlattice with CdTe QDs,4 as well as a three-dimensional crystal of themselves.5 In addition, linear chain-like assemblies of spherical nanoparticles have been demonstrated,[8] which were formed from the electrostatic dipoles of QDs[9] or by spin dipoles of magnetic nanoparticles.[10,11]

Modification of the surfactants on nanoparticles with functional ligands[12-14] or polymers[15,16] has also been shown to result in the formation of linear superstructures of nanoparticles upon the balancing of the forces of attraction and repulsion between the nanoparticles.[8] In the case of ligand modifications, the chemical nature of spherical nanoparticles plays a minor role in the formation of these linear chains. In contrast, anisotropic nanorods of gold, which were stabilized by polar surfactants, allowed for the selective attachment of non-polar polymeric ligands onto the terminal facets at the two ends of the nanorod, resulting in two non-polar patches connected by a polar nanorod in the center.[17,18] These end-functionalized nanorods were then polymerized into a

supracolloidal chain by increasing the polarity of the solvent around the nanorods, which generated directional attraction between the non-polar polymers at the ends of neighboring nanorods but lateral repulsion due to the polar surfactants on the nanorods.

This strategy of inducing directional attraction with orthogonal repulsion between nanoparticles to achieve a linear superstructure was applied to patched micelles of triblock terpolymers.[19,20] Polymeric colloidal nanoparticles, including polymerization-induced self-assemblies,[21-23] have shown various anisotropic structures[24-26] with nanoscale patches.[27-29] In particular, triblock terpolymers in a non-solvent for the central block formed micelles consisting of the insoluble core and the compartmentalized corona with polar patches and non-polar patches which were repulsive and attractive parts, respectively, during supracolloidal polymerization by increasing the polarity of the solvent.[19]

Recently, it was found that anisotropic patched micelles also can be induced from core-crosslinked micelles of diblock copolymers.[30] When the solvent is changed to be favorable to the cross-linked core, the central core is directly exposed to the solvent and the corona is rearranged into two patches. In other words, spherical micelles are converted to anisotropic micelles with the corona reorganized into two non-polar patches. From these anisotropic micelles,

supracolloidal polymer chains are induced by further increases in the polarity of the solvent.

If nanoparticles are encapsulated by block copolymer micelles which can form self-assembled linear chains, nanoparticles would be arranged linearly by supracolloidal polymer chain. In this chapter, we demonstrate linear arrangement of QDs directed by the supracolloidal polymer chain of block copolymer micelles in solution. We initially encapsulated green or red emitting QDs by diblock copolymers as a functional ligand capable of supracolloidal polymerization. In other words, QDs were selectively loaded into the cores of the uniform spherical micelles provided by diblock copolymers so that supracolloidal polymerization was insensitive to the size and type of QDs, and allowed for the suprachains to contain different QDs. After cross-linking the cores of micelle, supracolloidal polymer chains were induced by sequential changing the polarity of the solvent. Since each chain contained ether green- or red-emitting QDs, we successfully produced fluorescent supracolloidal chains functionalized with QDs. Furthermore, by combining micellar monomers containing green- and red-emitting QDs at monomeric and polymeric states, we were able to achieve the supracolloidal random and block chains with green and red emissions, which were directly observed by structured illumination microscopy(SIM).

4-2. Experimental Section

Materials

Polystyrene-b-poly(4-vinyl pyridine), PS(51)-b-P4VP(18), with a number average molecular weight of 51.0 kg/mol for PS and 18.0 kg/mol for P4VP and a polydispersity index (PDI) is 1.15, was purchased from Polymer Source, Inc.. We used green-emitting QDs of core-shell CdSe@ZnS capped with oleic acid (green QDs) whose synthetic procedure is described in the literature.[32] Red-emitting QDs of CdSe@ZnS (red QDs) were purchased from QD Solution Co, LTD. All other solvents and chemicals were purchased from Sigma-Aldrich and used as received.

Crosslinked PS(51)-b-P4VP(18) micelles with QDs

PS(51)-*b*-P4VP(18) (10.0 mg) and green QDs (2.5 mg) were dissolved in a mixed solvent system of chloroform (3.7 g) and THF (8.8 g) to yield a 0.1 wt% solution. 11-mercapto-1-undecanol (MCU) (1.0 mg, 4.9 μmol) was then added to this solution (12.5 g), followed by stirring at 40 ^{o}C for 12 h. Toluene (4.0 g) was slowly added by a syringe pump to this mixture at a rate of 2.0 ml/h to induce the formation of micelles. After mixing, the chloroform and THF were evaporated under reduced pressure and the solution (4.0 g) was diluted with toluene (8.5 g) to obtain a 0.1 wt% solution of QD-embedded micelles. To crosslink the P4VP cores, 1,4-dibromobutane (DBB) (2.7 mg, 12 μmol) was added to this solution

(12.5 g) containing PS(51)-*b*-P4VP(18) (10.0 mg), yielding a molar ratio of DBB to 4VP equal to 0.5, which can fully quarternize the 4VP units in the copolymer, followed by stirring at 45 ^{o}C for 48 h. PS(51)-*b*-P4VP(18) micelles containing red QDs were prepared employing a similar procedure where red QDs (1.0 mg) and MCU (0.2 mg, 1.0 μmol) were used.

Patched micelles with QDs

To produce colloidal monomers of patched micelles with QDs, the polarity of the solvent was changed by adding dimethylformamide (DMF) which is 9 times to toluene in weight, to a 0.1 wt% toluene solution of cross-linked PS(51)-*b*-P4VP(18) micelles containing QDs, resulting in a 0.01 wt% solution of colloidal monomers containing QDs with a reorganized corona of two PS patches.

Supracolloidal polymer chains of patched micelles with QDs

The polarity of the solvent was further increased to synthesize supracolloidal polymer chains from colloidal monomers of PS(51)-*b*-P4VP(18) micelles containing QDs. A mixture of DI water and anhydrous DMF (3:7 w/w) was added by a syringe pump at a rate of 10 ml/h to yield 15.0 wt% water in the final solution. The solution was stood without stirring at 30 ^{o}C for 48 h.

Supracolloidal random and block copolymer chains

To prepare supracolloidal random copolymer chains, two colloidal monomers containing green and red QDs independently were initially mixed in equal amounts. Then, a mixture of DI water and anhydrous DMF (3:7 w/w) was added by a syringe pump at a rate of 10 ml/h to the solution to obtain 15 wt% water in the final solution. The solution was kept standing without stirring at 30 °C for 48 hr. To synthesize supracolloidal block copolymer chains, two pre-polymerized chains containing green and red QDs independently were mixed in an equal amount. The mixed solution was kept standing without stirring at 30 °C for additional 24 hr.

Characterizations

Transmission electron microscopy (TEM) was performed on a Hitachi H-7600 at 100 kV. A TEM sample was prepared by dropping a solution of micelles or supracolloidal chains onto a carbon-coated TEM grid with removal of excess solvent using a filter paper. After drying in air, the TEM sample was exposed to iodine or ruthenium tetroxide vapor to stain P4VP or PS. UV-Vis absorption spectra were recorded on a Varian Cary-5000 spectrophotometer. Steady-state fluorescence was measured on an Acton SpectraPro with a He-Cd laser (325 nm) as the excitation source. Dynamic light scattering was performed using a DLS-8000 instrument (Otsuka Electronics Co, Ltd) with a fixed scattering angle of 90°.

Structured illumination microscopy (SIM) was performed on a dried sample prepared by spin-coating (6000 rpm, 60 s) a solution of supracolloidal chains onto a glass substrate using an Elyra PS1 microscope system (Carl Zeiss) equipped with an EMCCD camera (Andor Technology) at the National Center for Inter-University Research Facilities. Excitation with an Argon laser at 488 nm was used with emission filters (495~550 nm for green QDs and 570~620 nm for red QDs). A SIM image was acquired from z-stacks containing 5 phase-shifts and 3 rotations per z-slice (100 nm interval) and processed with Zen software (Carl Zeiss). For multicolor imaging, channels were aligned using a multispec calibration slide (170 nm beads, Carl Zeiss) with the channel alignment program in Zen software.

4-3. Results and Discussion

We first employed green-emitting QDs (green QDs) comprised of core-shell CdSe@ZnS capped with oleic acid,[32] which are shown in Fig. 1a. The shape of these QDs is not completely spherical due to the presence of a thick ZnS shell that made a relatively large diameter of 9.4 nm (±0.6 nm) but was necessary for stable green emission at 500 nm (Figure 4-1).[33] These green QDs were incorporated into the micelles of polystyrene-b-poly(4-vinyl pyridine) (PS(51)-b-P4VP(18), the number in the parenthesis is a number-average molecular weight in kg/mol), which formed self-assembled linear chains. To embed the QDs selectively in the P4VP cores, we induced the formation of micelles consisting of the PS corona and the P4VP core in the presence of QDs. A small amount of 11-mercapto-1-undecanol was added to promote selective loading of QDs into the P4VP cores.[34] First, PS(51)-b-P4VP(18) and QDs were homogenously dissolved in a mixture of chloroform and THF. Then, toluene, a PS-selective solvent, was added to this solution. After evaporation of chloroform and THF, we obtained a toluene solution of PS(51)-b-P4VP(18) micelles with QDs.

Figure 4-2a is the transmission electron microscopy (TEM) image of PS(51)-b-P4VP(18) micelles with QDs on a carbon-coated TEM grid after the removal of toluene. Since both PS and P4VP blocks are glassy at room temperature, the spherical shape of the micelle was well preserved in the image. The PS coronas

appear blurry bright grey but the P4VP cores (~27 nm in diameter) are clearly discernible as dark grey spheres because of iodine staining. The diameter of these micelles was ~80 nm as measured by dynamic light scattering (DLS) (Figure 4-3a), a value that represents the micellar size in solution, prior to solvent evaporation. In these P4VP cores, one or two QDs can be observed as black dots, indicating successful loading of QDs in the cores of micelles. From a larger TEM image, the average number of QDs per micelle was calculated to be 1.5. We note that the portion of empty micelles without QDs was about 8.5% (Figure 4-4a).

We also embedded red-emitting QDs (red QDs) comprised of CdSe@ZnS, which has a maximum emission intensity at 605 nm (Figure 4-1), into PS(51)-b-P4VP(18) micelles following the same procedure as that described earlier. Red QDs themselves are shown in Figure 4-2d which are smaller than green QDs because of a thinner shell of red QDs. The diameter of red QDs is 6.5 nm (±1.1 nm), and therefore they can be distinguished from the green QDs in the TEM images shown on the same scale (Figure 4-2a and 2d). After incorporation of red QDs into the micelles of PS(51)-b-P4VP(18), the QDs could can be found selectively in the dark P4VP cores (~23 nm in diameter) (Figure 4-2e), implying that they were well loaded in the cores of micelles. The diameter of the micelles with red QDs was ~77 nm, as measured by DLS (Figure 4-3b), a size that is not significantly different than the micelles embedded with green QDs. The average

number of red QDs per micelle was calculated to be 2.1 (Figure 4-4b), however, a larger value than that of green QDs (1.5), primarily due to the smaller size of the red QDs. The portion of empty micelles without QD decreased to 4.8% (Figure 4-4b). Thus, we were able to incorporate green and red QDs independently into PS(51)-b-P4VP(18) micelles. It is worth noting that we can differentiate micelles with red QDs from those with green QDs in a TEM image, not only by the diameter of QDs but also by the number of QDs per micelle.

By crosslinking the P4VP cores with 1,4-dibromobutane (DBB) and changing the polarity of the solvent upon the addition of DMF, spherical micelles of PS(51)-b-P4VP(18) encapsulating QDs can be converted into anisotropic micelles having two separated PS patches and the central P4VP core directly exposed to DMF. The two images in Figure 4-5a and b clearly show the rearranged structures of PS(51)-b-P4VP(18) micelles. In the TEM image obtained after staining P4VP with iodine (Figure 4-5a), we can observe two separated PS patches with the P4VP core between them. The two PS patches are noticeably visualized by selective staining PS with ruthenium tetraoxide in the TEM image of Figure 4-5b, which shows an anisotropic micellar structure of two spherical PS patches connected by the P4VP core. Remarkably QDs remained in the P4VP core after rearrangement, and can be seen as black dots in the middle of the anisotropic micelles in both left and right images of Fig. 1c. From these TEM

images, we found that the average number of QDs per micelle was not affected during the rearrangement of the PS coronas. We note that some of micelles had asymmetric PS patches.

Segregation of the PS corona, initiated by exposure of the crosslinked P4VP core to favorable DMF, depends on a volume fraction of the PS corona to the P4VP core. A small fraction of the corona can induce three, instead of two, separated patches. Since the incorporation of QDs into the P4VP core resulted in the formation of a larger core volume (a smaller corona fraction) than that of pristine micelles without QDs, we observed many micelles having three PS patches after rearrangement but intentionally suppressed them by reducing the ratio of DMF to toluene used when compared to that used for pristine micelles in an attempt to pursue linear supracolloidal polymerization with fewer branches and networks caused by micelles with three patches. We are currently investigating this patch formation and its dependence on the proportion of the corona block and supracolloidal network formation with micelles having three patches.

Patched micelles with red QDs were also induced by crosslinking the P4VP core and changing the polarity of the solvent using DMF. TEM images in Figure 4-5c and d show these rearranged micelles. Two PS patches in the corona can be clearly seen after staining the samples with ruthenium tetraoxide (Figure 4-5d),

whereas QDs in the central P4VP core can be counted in the image stained with iodine (Figure 4-5c). The average number of red QDs per micelle was not changed by the patch formation as observed in TEM images.

For the linear polymerization of colloidal nanoparticles, directional attraction between nanoparticles with repulsion orthogonal to this attraction is necessary.[20] In the rearranged micelles, two PS patches, which are non-polar, can act as attractive sections when the solvent becomes more polar by the addition of water. In contrast, the central P4VP core, which is polar and directly exposed to the solvent, can serve as a repulsive section to avoid non-directional aggregation. To polymerize the patched micelles with QDs, we added water, which was diluted with DMF, to a solution of the rearranged micelles containing green QDs. By addition of water, the non-polar PS patches became unfavorable to the contact with water so that attraction between the PS patches of neighboring micelles was exerted, leading to the polymerization between the patched micelles. In Figure 4-6a, we can confirm the formation of a supracolloidal polymer chain. The inset shows an entire polymer chain with a length of ~6.5 μm (a fully enlarged image can be seen in Figure 4-7) and the boxed area (in blue) corresponds to the enlarged image of Fig 4-6a. The TEM image of Figure 4-6a clearly shows an alternating structure of the connected PS patches and the P4VP cores in which we can find one or two QDs. The number of micellar cores in the polymer was

counted from the image (Figure 4-7) to be 180, which corresponds to a degree of polymerization (DP) of the chain.

A solution of these supracolloidal chains with green QDs emitted the green light centered at 519 nm, as shown in Figure 4-6b, which is slightly red-shifted compared to that of the pristine QDs. In addition, we directly investigated an individual chain with SIM, one of super-resolution fluorescence microscopic techniques.[35] A SIM image of Figure 4-6c clearly shows a green-emitting chain with a length of ~5.0 μm. In a large-area image (Figure 4-8), more chains with various lengths of green emission are visible. Emission of each chain seems to have an intensity variation along the chain, presumably because the feature size of the repeating unit containing QDs is smaller than the resolution limit of SIM (~120 nm)[36] so that the intensity variation cannot be directly correlated to the micellar unit. Nevertheless, we can find chains having various conformations such as extended chains and coils (Figure 4-8).

By repeating the polymerization process with the patched micelles with red QDs (Figure 4-6f), we also synthesized red-emitting supracolloidal polymer chains. In Figure 4-6d, we again confirmed the formation of a supracolloidal chain consisting of alternating PS patches and P4VP cores. The length of an entire chain (Figure 4-9) is ~4.5 μm with a DP of 116. However, most P4VP cores have more than one QD, which will make it possible to verify the repeat unit of red

QDs from a TEM image later. Supracolloidal chains containing red QDs obviously generated the red emission at 605 nm (Fig. 2e). A red-emitting individual chain was also verified in a SIM image (Figure 4-6f). More red-emitting chains with various lengths are visible in a large-area image (Figure 4-10). We note that the wavelength of the maximum intensity was the same as that of pristine red QDs (Figure 4-6e) and a portion of short chains was relatively high in comparison with the case of the green-emitting chains (Figure 4-8 and 10).

Since we had two differently emitting colloidal monomers of the rearranged micelles containing green and red QDs, the synthesis of supracolloidal random and block copolymer chains was demonstrated simply by mixing at monomeric and polymeric states.[30] For supracolloidal random copolymer chains, two colloidal monomers containing green and red QDs independently were initially mixed in an equal amount then polymerized by the addition of water. Figure 4-11a shows a supracolloidal random copolymer consisting of rearranged micelles containing green and red QDs. A whole chain in the inset is also given in Figure 4-12. We differentiated between the cores containing green QD by marking grey false colors, respectively, with our best efforts by enlarging the image enough for clear view on the size of QDs. As marked, a random distribution of green and red QDs along the chain confirmed the synthesis of a supracolloidal random copolymer chain. Empty micelles without QDs are not colored.

We also verified the formation of supracolloidal random copolymers by fluorescence analysis on both a solution and individual chains. As shown in Figure 4-11b, both green and red emissions at 520 and 605 nm, respectively, with almost equal intensity were observed, resulting in an orange-coloured fluorescent solution (as shown in the inset photo). This observation indicates that no energy transfer occurs between the green and red QDs which is as expected because of good separation between the QDs by the connected PS patches. A random copolymer chain was also observed in the SIM image of Figure 4-11c, in which green and red emissions are randomly distributed along a single linear chain with a length of ~3.1 μm. We note that because of the resolution limit of SIM, the variation in emitting colour along the chain cannot directly explain the detailed structure of a random copolymer chain.[36]

A supracolloidal block copolymer was also synthesized by blending two pre-polymerized chains containing green and red QDs independently. Since two ends of the supracolloidal chains are the PS patches, connections between chains can be induced regardless of the type of chains having green or red QDs, although the number of blocks, i.e., homopolymers connected, is arbitrary. Two homopolymer chains functionalized with green or red QDs independently were mixed in equal amounts and left to stand for 24 h. Figure 4-11d shows a di-block chain consisting of two homopolymers with green QDs (left side) and red QDs (right side), which

is clearly visible in an enlarged image (Figure 4-13). A solution of supracolloidal block chains showed orange-colored fluorescence with simultaneous green and red emission (Figure 4-11e), which is identical to that from a solution of supracolloidal random copolymer chains. However, nanoscale fluorescence from a block copolymer chain was dramatically different as shown in the SIM image of a tetra-block chain of ~8 μm long (Figure 4-11f) which consists of two green-emitting and two red-emitting blocks, thereby confirming the synthesis of block copolymer chains.

4-4. Conclusion

In conclusion, we were able to arrange QDs with supracolloidal chains. We encapsulated QDs into the P4VP cores of PS-b-P4VP diblock copolymer micelles which were then converted to micelles consisting of two PS patches connected by a crosslinked P4VP core. Since PS-b-P4VP diblock copolymers provided uniform micelles regardless of the type and size of the QDs, green- and red-emitting QDs were incorporated into the supracolloidal chains which were polymerized from patched micelles containing QDs. Furthermore, the polymerization of colloidal monomers of patched micelles was insensitive to the QDs loaded in the core of the micelles so that we were able to synthesize supracolloidal random and block chains simultaneously emitting two colors from two different QDs. These supracolloidal chains capable of multiple emissions are of potential use in many areas such as in optical and diagnostic applications. Moreover, this approach demonstrated here to arrange linearly by supracolloidal polymerizations are universally applicable to various nanoparticles of metals and oxides beyond QDs for numerous applications.

4-5. References

[1] C. B. Murray, C. R. Kagan and M. G. Bawendi, *Annu. Rev. Mater. Sci.*, 2000, **30**, 545.

[2] D. Vanmaekelbergh, *Nano Today*, 2011, **6**. 419.

[3] Y. Shirasaki, G. J. Supran, M. G. Bawendi, V. Bulovic, *Nat. Photon.*, 2013, **7**. 13.

[4] Z. Chen, J. Moore, G. Radtke, H. Sirringhaus and S. O'Brien, *J. Am. Chem. Soc.*, 2007, **129**, 15702.

[5] C. B. Murray, C. R. Kagan, M. G. Bawendi, *Science*, 1995, **270**, 1335.

[6] C. R. Kagan and C. B. Murray, *Nat. Nanotechnol.*, 2015, **10**, 1013.

[7] M. Grzelczak, J. Vermant, E. M. Furst and L. M. Liz-Marzán, *ACS Nano*, 2010, **4**, 3591.

[8] L. J. Hill, N. Pinna, K. Char, J. Pyun, *Prog. Polym. Sci.*, 2015, **40**, 85.

[9] Z. Y. Tang, N. A. Kotov, M. Giersig, *Science*, 2002, **297**, 237.

[10] L. J. Hill, N. E. Richey, Y. Sung, P. T. Dirlam, J. J. Griebel, E. Lavoie-Higgins, I.-B. Shin, N. Pinna, M.-G. Willinger, W. Vogel, J. J. Benkoski, K. Char and J. Pyun, *ACS Nano*, 2014, **8**, 3272.

[11] N. G. Pavlopoulos, J. T. Dubose, N. Pinna, M.-G. Willinger, K. Char and J. Pyun, *Angew. Chem. Int. Ed.*, 2016, **55**, 1787.

[12] R. M. Choueiri, A. Klinkova, H. Thérien-Aubin, M. Rubinstein and E.

Kumacheva, *J. Am. Chem. Soc.*, 2013, **135**, 10262.

[13] J. Lai, Y. Xu, X. Mu, X. Wu, C. Li, J. Zheng, C. Wu, J. Chen and Y. Zhao, *Chem. Commun.*, 2011, **47**, 3822.

[14] C. Xi, P. F. Marina, H. Xia and D. Wang, *Soft Matter*, 2015, **11**, 4562.

[15] Y. Kang, K. J. Erickson and T. A. Taton, J. Am. Chem. Soc., 2005, **127**, 13800.

[16] H. Wang, L. Chen, X. Shen, L. Zhu, J. He and H. Chen, *Angew. Chem. Int. Ed.*, 2012, **51**, 8021.

[17] Z. Nie, D. Fava, E. Kumacheva, S. Zou, G. C. Walker and M. Runinstein, *Nat. Mater.*, 2007, **6**, 609.

[18] K. Liu, Z. Nie, N. Zhao, W. Li, M. Rubinstein and E. Kumacheva, *Science*, 2010, **329**, 197.

[19] A. H. Gröschel, F. H. Schacher, H. Schmalz, O. V. Borisov, E. B. Zhulina, A. Walther and A. H. E. Müller, *Nat. Commun.*, 2012, **3**, 710.

[20] A. H. Gröschel, A. Walther, T. I. Löbling, F. H. Schacher, H. Schmalz and A. H. E. Müller, *Nature*, 2013, **503**, 247.

[21] A. Blanazs, J. Madsen, G. Battaglia, A. J. Ryan and S. P. Armes, *J. Am. Chem. Soc.*, 2011, **133**, 16581.

[22] S. Boissé, J. Rieger, K. Belal, A. Di-Cicco, P. Beaunier, M. H. Li and B. Charleux, *Chem. Commun.*, 2010, **46**, 1950.

[23] J.-T. Sun, C.-Y. Hong and C.-Y. Pan, *Soft Matter*, 2012, **8**, 7753.

[24] Z. M. Hudson, D. J. Lunn, M. A. Winnik and I. Manners, *Nat. Commun.*, 2014, **5**, 3372.

[25] Q. Chen, S. C. Bae and S. Granick, *Nature*, 2011, **469**, 381.

[26] Y. Wang, Y. Wang, D. R. Breed, V. N. Manoharan, L. Feng, A. D. Hollingsworth, M. Weck and D. J. Pine, *Nature*, 2012, **491**, 51.

[27] J. Du and R. K. O'Reilly, *Chem. Soc. Rev.*, 2011, **40**, 2402.

[28] A. H. Gröschel and A. H. E. Müller, *Nanoscale*, 2015, **7**, 11841.

[29] D. J. Lunn, J. R. Finnegan and I. Manners, *Chem. Sci.*, 2015, **6**, 3663.

[30] J. H. Kim, W. J. Kwon and B. H. Sohn, *Chem. Commun.*, 2015, **51**, 3324.

[31] Y. Mai and A. Eisenberg, *Chem. Soc. Rev.*, 2012, **41**, 5969.

[32] W. K. Bae, K. Char, H. Hur and S. Lee, *Chem. Mater*., 2008, **20**, 531.

[33] B. O. Dabbousi, J. Rodriguez-Viejo, F. V. Mikulec, J. R. Heine, H. Mattoussi, R. Ober, K. F. Jensen and M. G. Bawendi, *J. Phys. Chem. B*, 1997, **101**, 9463.

[34] Q. Li, J. He, E. Glogowski, X. Li, J. Wang, T. Emrick, T. P. Russell, *Adv. Mater.*, 2008, **20**, 1462.

[35] A. Jost and R. Heintzmann, *Annu. Rev. Mater. Res.*, 2013, **43**, 261.

[36] M. G. L. Gustafsson, *J. Microsc.*, 2000, **198**, 82.

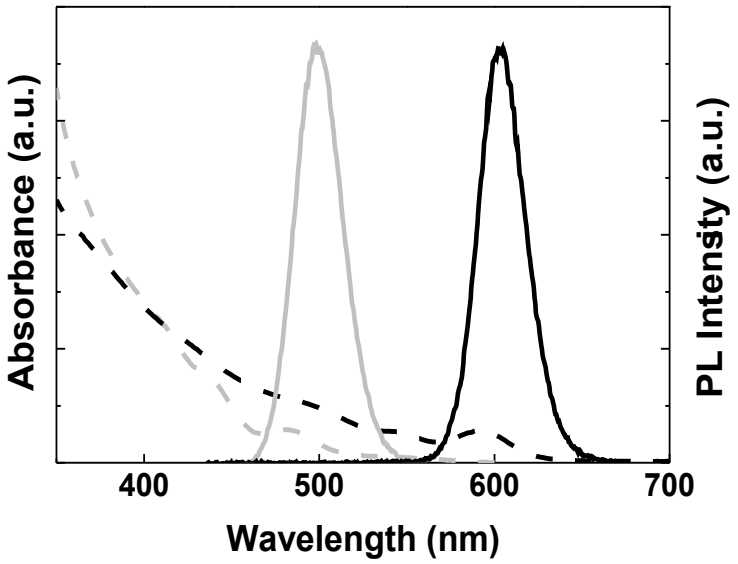

Figure 4-1. UV-Vis (dashed) and photoluminescence (solid) spectra of green QDs (grey) and red QDs (black).

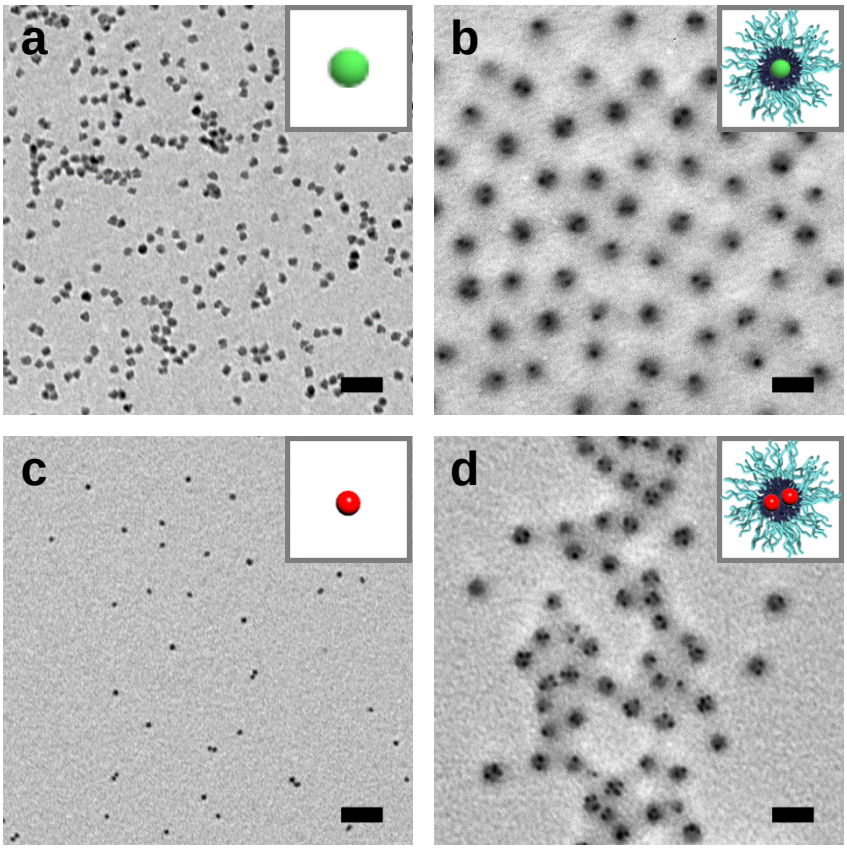

Figure 4-2. TEM Images: (a) green QDs; (b) spherical micelles with green QDs; (c) red QDs; (d) spherical micelles with red QDs. All scale bars are 50 nm.

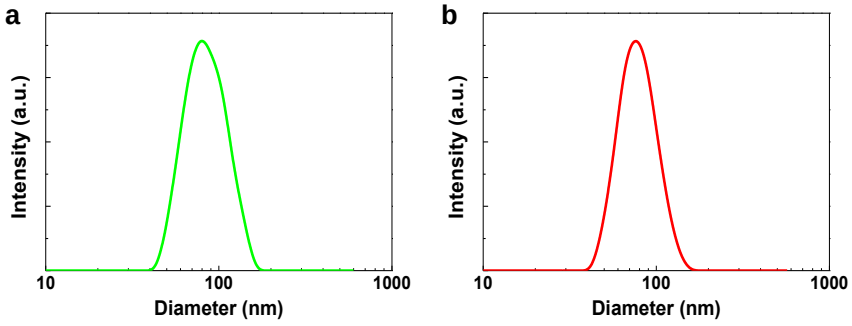

Figure 4-3. Dynamic light scattering (DLS) results of PS-b-P4VP micelles with QDs: (a) micelles with green QDs; (b) micelles with red QDs.

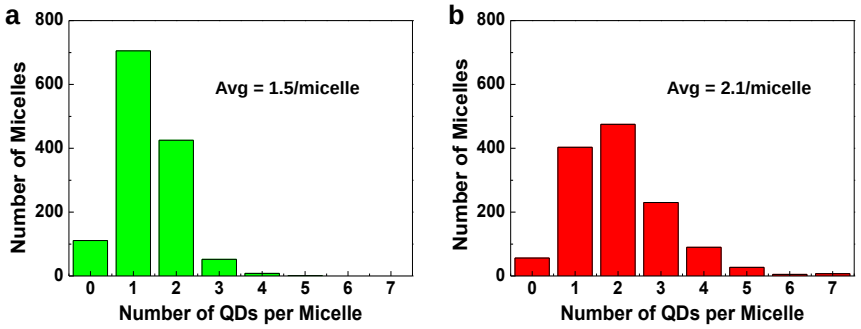

Figure 4-4. Histograms of the number of QDs per micelle: (a) green QDs; (b) red QDs.

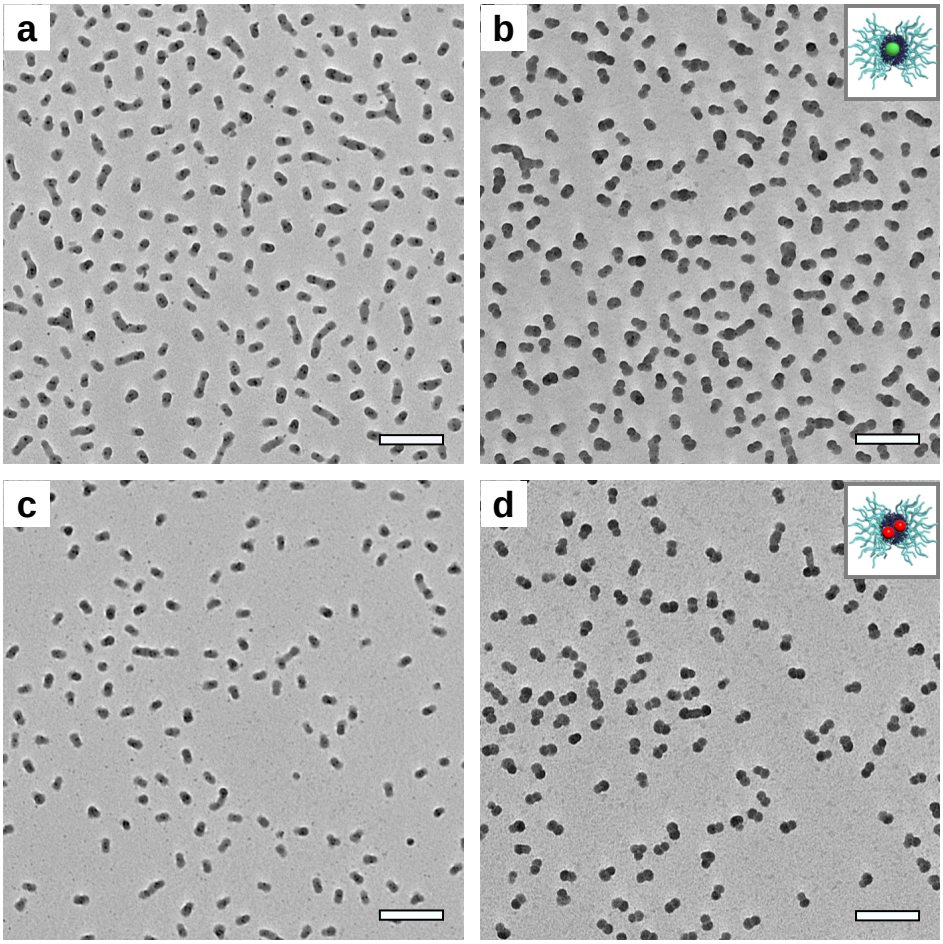

Figure 4-5. TEM images of patched micelles with green QDs (a,b), and with red QDs (c,d). Left images (a,c) were stained with I_2 whereas right images were stained with RuO_4. All scale bars are 100 nm.

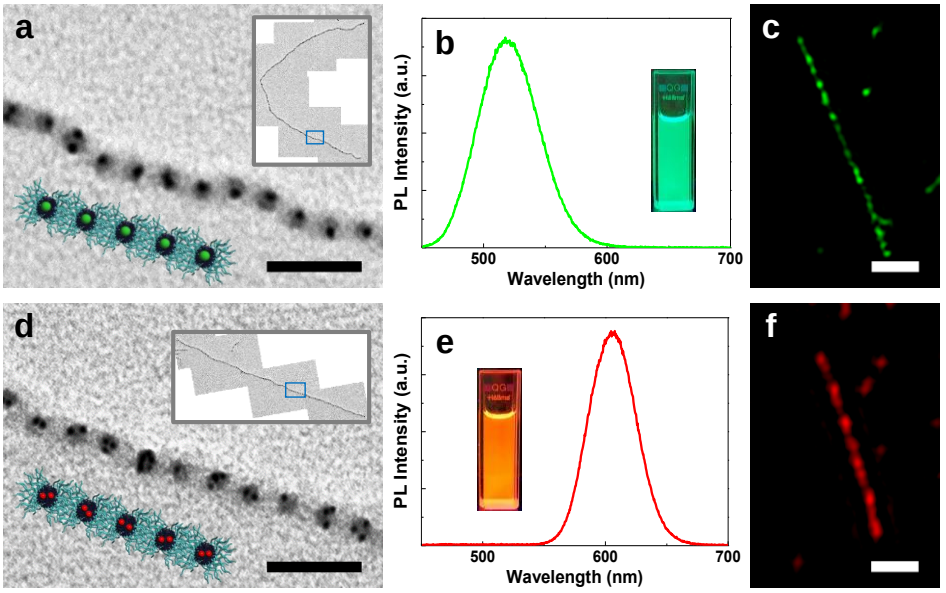

Figure 4-6. Supracolloidal chains functionalized with green QDs (top row) and red QDs (bottom row): (a)(d) TEM images; (b)(e) PL spectra with photos; (c)(f) SIM images. TEM images correspond to the marked areas in the insets showing whole chains. The scale bars in TEM and SIM images are 100 nm and 1 μm, respectively.

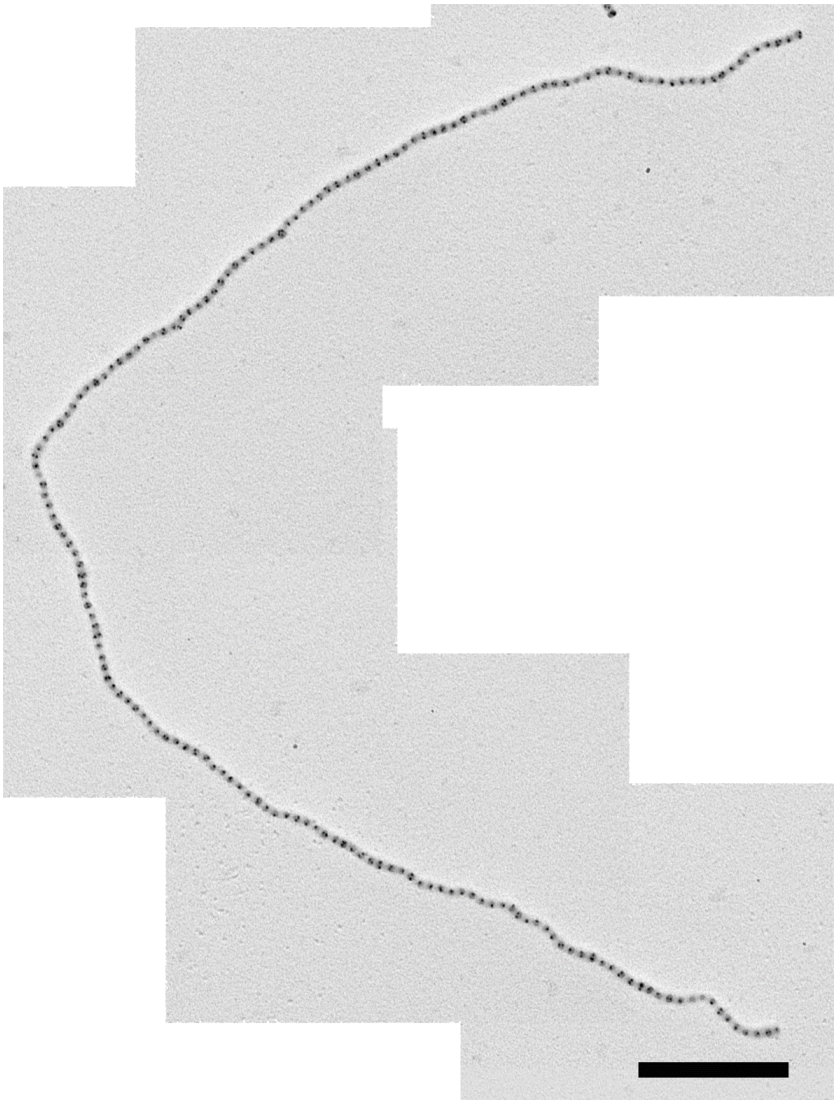

Figure 4-7. TEM image of a supracolloidal polymer chain with green QDs shown in the inset of Figure 4-6a. The scale bar is 500 nm.

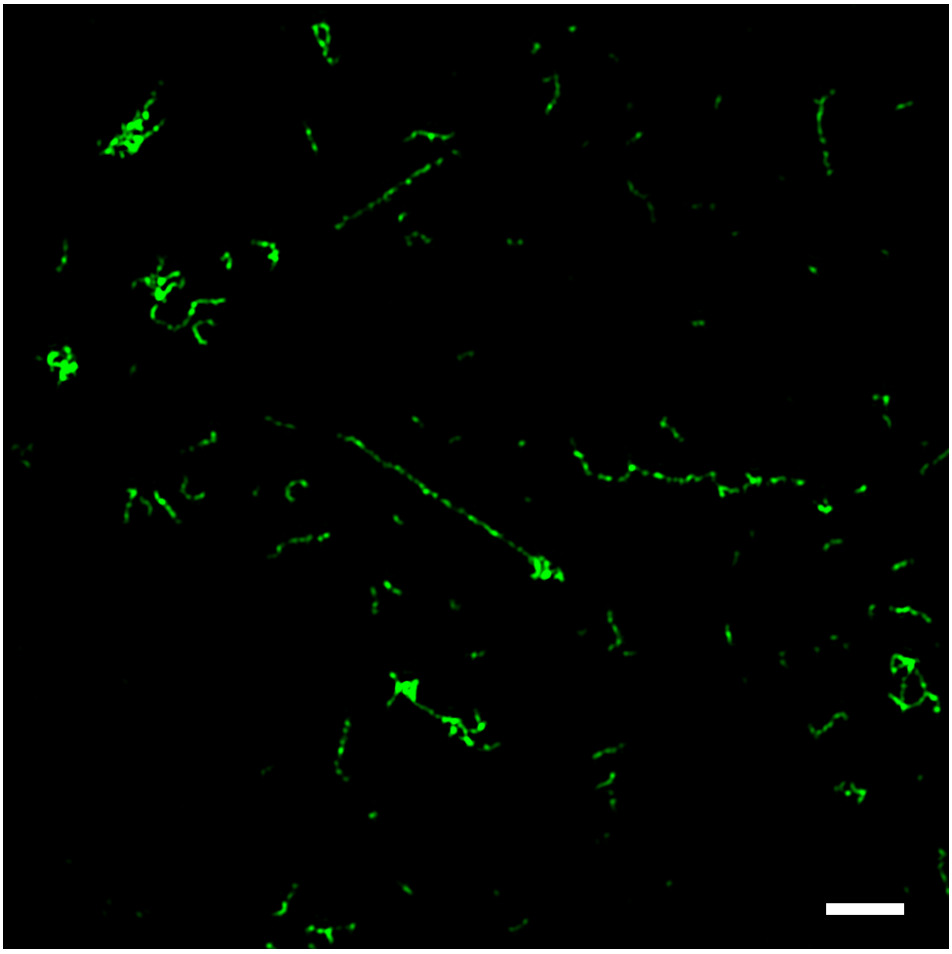

Figure 4-8. Large-area SIM image of supracolloidal chains functionalized with green QDs. The scale bar is 1 μm.

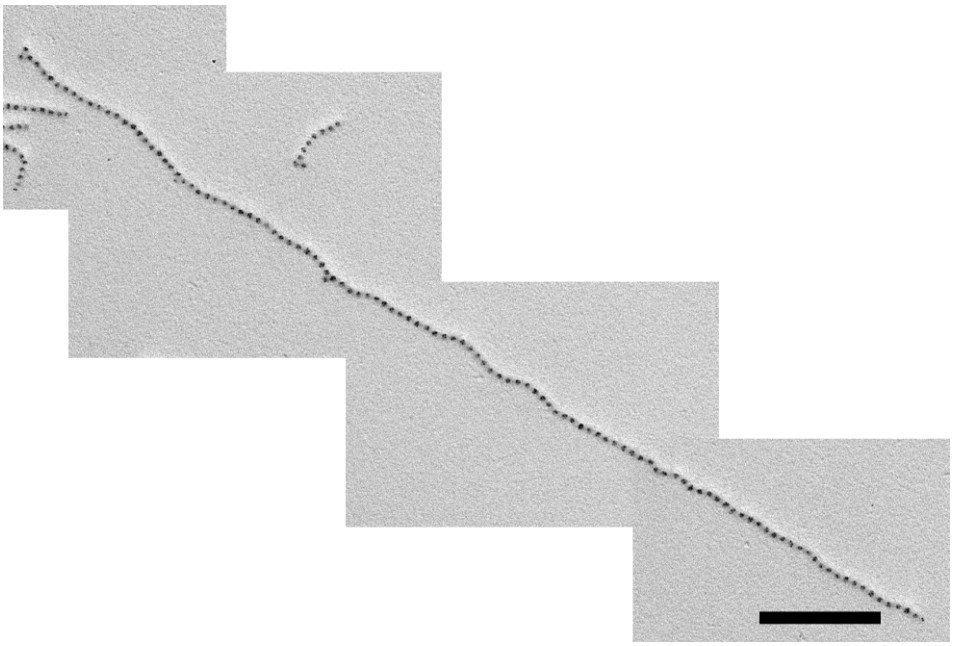

Figure 4-9. TEM image of a supracolloidal polymer chain with red QDs shown in the inset of Figure 4-6(d). The scale bar is 500 nm.

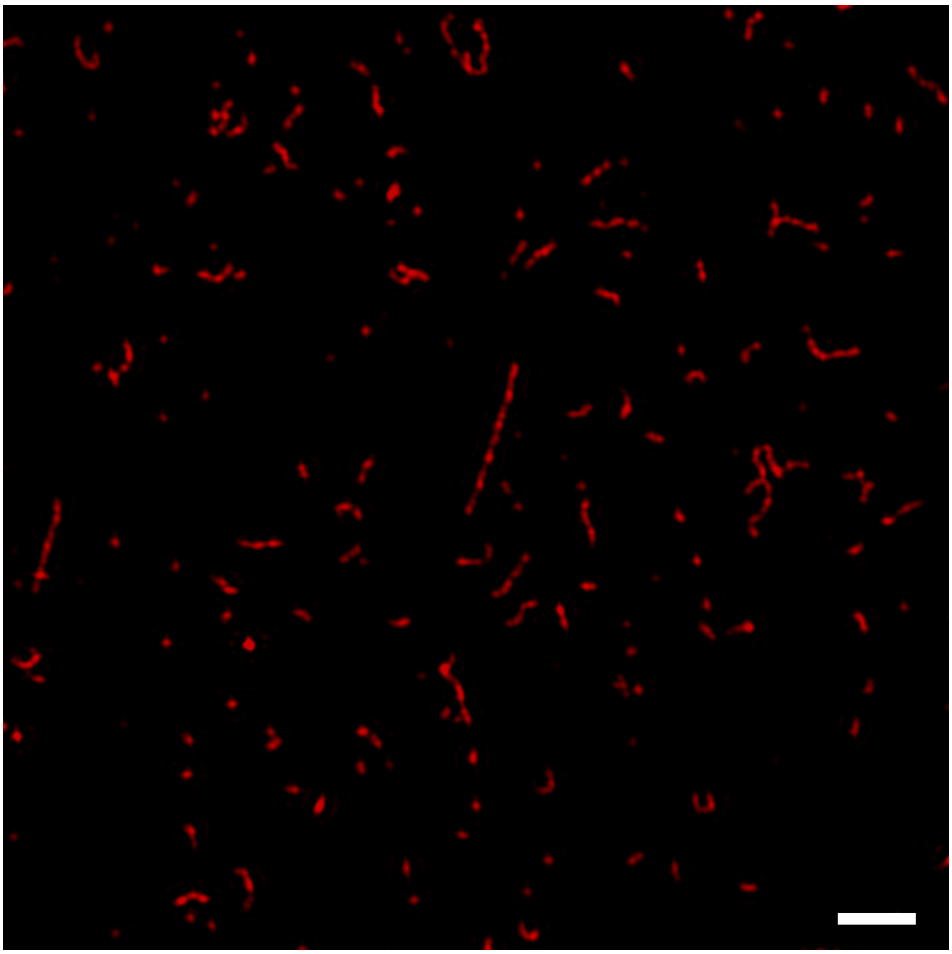

Figure 4-10. Large-area SIM image of supracolloidal chains functionalized with red QDs. The scale bar is 1 μm.

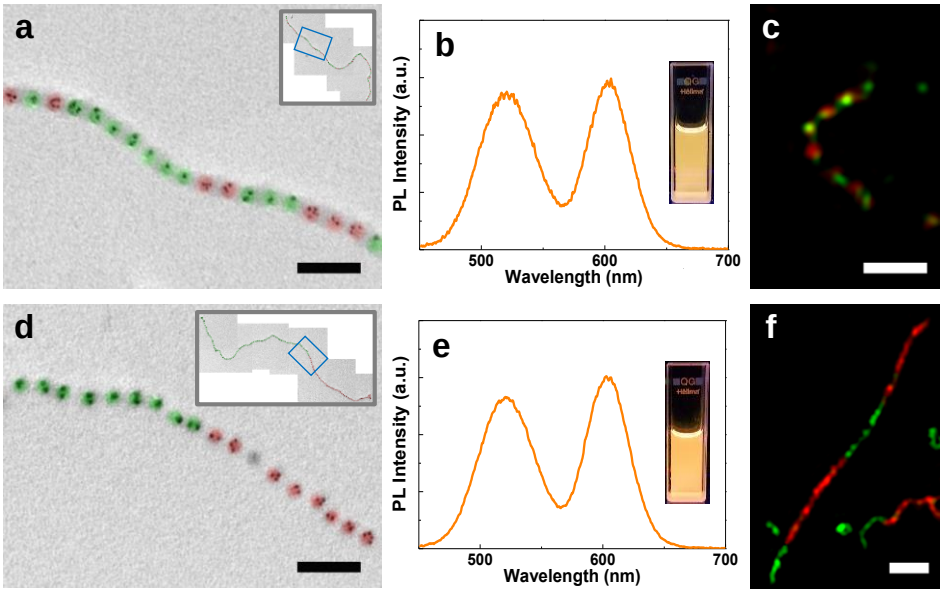

Figure 4-11. Supracolloidal random (top row) and block (bottom row) copolymer chains functionalized with green QDs and red QDs: (a)(d) TEM images; (b)(e) PL spectra with photos; (c)(f) SIM images. TEM images correspond to the marked areas in the insets showing whole chains. Green and red false colors are applied to the cores containing green and red QDs, respectively. The scale bars in TEM and SIM images are 100 nm and 1 μm, respectively.

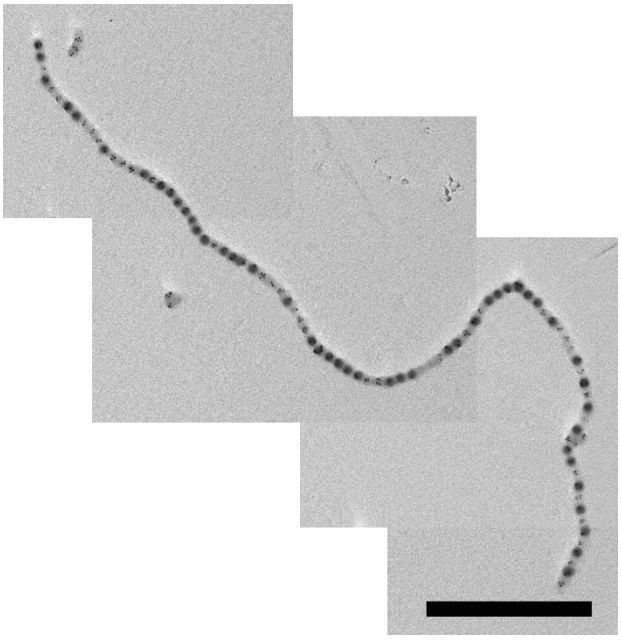

Figure 4-12. TEM image of a supracolloidal random copolymer chain with green and red QDs shown in the inset of Figure 4-11(a). Grey false colors are applied to the cores containing green QDs. The scale bar is 500 nm.

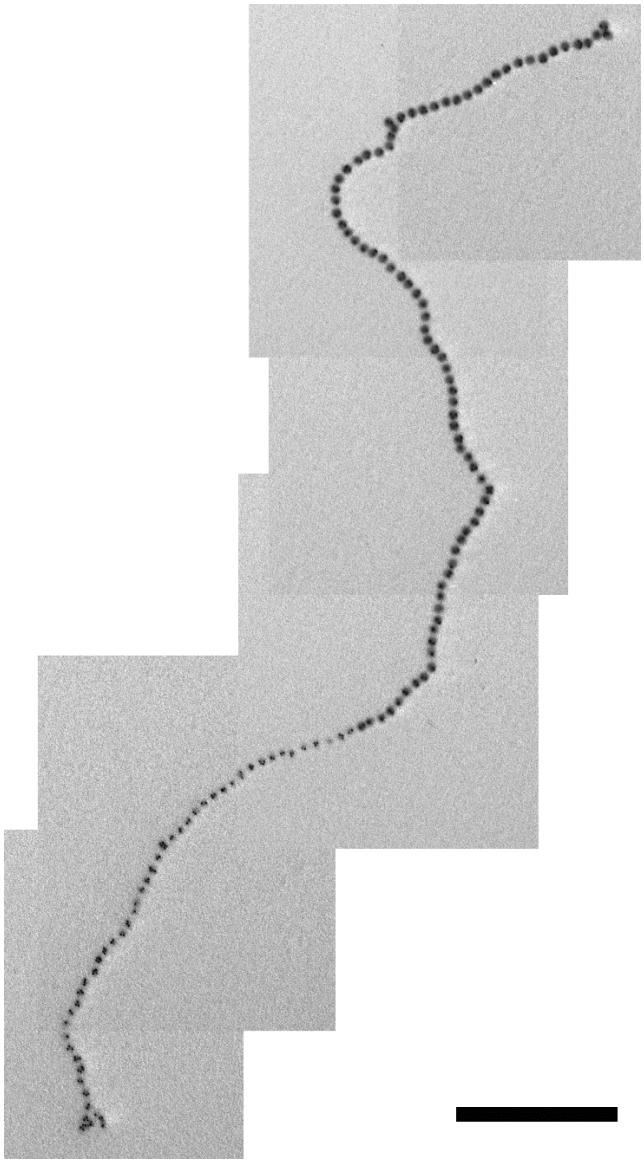

Figure 4-13. TEM image of a supracolloidal block copolymer chain with green and red QDs shown in the inset of Figure 4-11(d). Grey false colors are applied to the cores containing green QDs. The scale bar is 500 nm.

국문요약

블록공중합체 나노구조에 의한 양자점의 배열 제어에 관한 연구

채승용

화학부 고분자 전공

서울대학교 대학원

구형의 금속, 산화금속 및 반도체로 이루어진 나노입자는 벌크 상태는 볼 수 없는 독특한 특성을 가지고 있기 때문에 차세대 소재로써 연구되어 왔다. 이와 같은 구형 나노입자는 최근 제조 기술의 발전으로 균일한 크기와 형태로 제조가 가능해짐에 따라, 용액상 혹은 고체상에서의 입자 간 배열에 대한 관심이 증폭되고 있으며, 특히 배열된 입자 간 상호작용에 의하여 개개의 나노입자와는 다른 특성이 관찰되기 때문에 이를 이용하려는 연구가 활발히 진행되고 있다. 양자점의

결정 구조의 제조가 보고된 이래로 단일 혹은 이중 이상의 나노입자로 이루어진 다양한 형태의 밀집구조가 연구되었으며, 이제는 단순한 밀집구조를 넘어 복잡한 구조의 나노입자 배열이 연구되고 있다.

나노입자의 배열은 전자 빔 혹은 광자 리소그래피에 의한 하향식 방법으로 얻어질 수 있다. 하지만 일반적인 리소그래피 기술에 의한 배열은 기판 위의 2차원적 평면에서만 유효하다는 한계를 가지고 있다. 반면 자기조립 구조를 가지는 물질에 의해 형성된 나노구조를 형판으로 하여 나노입자를 배열 할 수 있다면 상향식으로 1차원, 2차원 뿐만 아니라 3차원의 정렬된 배열을 구현할 수 있기 때문에 하향식의 한계를 극복할 수 있는 대안으로 부각되고 있다. 특히 둘 혹은 그 이상의 다른 화학적 구조를 가진 고분자 사슬로 구성된 블록공중합체는 고체상 혹은 용액상에서 자기조립에 의한 장거리 질서를 가진 정렬된 나노구조를 형성하기 때문에 나노입자의 배열 제어를 위한 이상적인 재료이다.

본 연구는 이중블록공중합체 나노구조를 통하여 양자점의 공간적 배열을 제어하는 데에 목적을 두었다. 블록공중합체 나노구조를 따라 양자점이 배열되기 위해서는 이중블록공중합체의 한 블록과 양자점 간의 선택적인 상용성이 요구된다. 이러한 상용성을 부여하기 위하여

이중블록공중합체의 특정 블록 혹은 양자점의 표면에 강한 상호 작용을 가능케 하는 기능기를 도입하였다. 이를 통해 양자점과 블록공중합체로 이루어진 복합 필름 내에서 블록공중합체 나노구조에 의한 양자점의 배열의 구현되었다. 또한 용액 상에서도 양자점이 이중블록공중합체 마이셀의 코어에 선택적인 도입이 이루어졌으며, 이중블록공중합체 마이셀이 형성하는 선형의 콜로이드 고분자 사슬을 통해 배열이 이루어졌다. 더 나아가 유기 형광체 혹은 다른 종류의 양자점과의 조합을 통하여 블록공중합체 나노구조에 의해 제어된 다중 형광특성을 구현할 수 있었다.

제 1장에서는 블록공중합체의 고체상 혹은 용액상에서 형성하는 자기조립 나노구조에 대하여 개괄적으로 서술하였다. 기능성 블록공중합체를 위한 합성 방법 및 후중합 반응에 관하여 간략히 소개하였다.

제 2장에서는 블록공중합체와 양자점으로 구성된 복합체 필름 내에서 블록공중합체의 판상형 나노구조를 따라 제어된 양자점의 배열을 다루었다. 블록공중합체가 양자점을 위한 고분자 매트릭스로서 배열을 할 수 있도록 하기 위하여, 반응성의 블록을 가진 블록공중합체를 합성하고, 후중합 반응에 의해 양자점과 강한 결합을 할 수 있는 티올기로 기능화하였다. 스핀코팅에 의하여 제조된 다양한 두께의 복합체 박

막 내에서 용매 증기 어닐링을 통하여 배향이 제어된 판상형의 나노구조를 유도하였으며, 나노구조를 따라 양자점이 효과적으로 배열되었음을 확인하였다. 또한 용매 캐스팅에 의해 제조된 수마이크로 두께의 프리스탠딩 필름에서도 무작위적 배열을 가진 판상형 나노구조 내에 양자점이 효과적인 배열을 하였음을 확인하였다.

제 3장에서는 2장에서 다루었던 티올 기능화된 블록공중합체와 양자점에 더하여 유기형광체로 기능화된 블록공중합체를 혼합하여, 블록공중합체 나노구조 내에 이종의 형광체를 동시 도입 및 배열하는 연구를 다루었다. 티올 기능화된 블록공중합체와 형광 기능화된 블록공중합체는 다른 종류의 기능기를 소량 가지고 있지만 화학적으로 동일한 기본적인 구조를 가지도록 하여 혼합 시 거대 상분리 없이 하나의 나노구조를 형성하도록 하였다. 2장에서 사용된 블록공중합체의 반응성 블록에 후중합 반응을 통하여 유기형광체를 결합하였으며, 이를 가지고 제조된 박막 내에서 유기 형광체로 기능화된 판상형 나노구조가 동일하게 형성됨을 확인하였다. 양자점과 각각의 기능화된 블록공중합체가 혼합된 복합체 박막 필름에서 형성된 판상형 나노구조의 한 블록 내에 양자점과 유기형광체가 동시에 선택적으로 도입되었으며, 나노구조 내에 제한되어 수나노 거리 안에 위치한 양자점과 유기형광체

사이의 FRET (Fluorescent Resonance Energy Transfer) 현상을 관찰하였다.

제 4장에서는 용액상에서 형성된 블록공중합체 마이셀을 단량체로 하여 형성된 콜로이드 고분자 사슬에 의한 양자점의 배열에 관하여 서술하였다. 녹색과 적색의 발광을 하는 양자점들은 먼저 표면의 개질을 통해 코어를 형성하는 블록과 수소결합이 가능하도록 하였으며, 이를 통해 블록공중합체 마이셀의 가교된 코어에 효과적으로 도입하였다. 양자점이 도입된 구형의 마이셀은 용매의 극성 조절을 통하여 2개의 패치를 가진 이방성의 콜로이드 구조로 변형되며, 추가적인 용매의 극성 조절을 통해 선형의 고분자 사슬을 형성함을 확인하였다. 또한 두 가지의 양자점이 각각 도입된 마이셀을 패치 입자 혹은 콜로이드 사슬 단계에서 혼합하는 방법을 통해 녹색과 적색의 발광을 동시에 가지는 랜덤 혹은 블록공중합 형태의 콜로이드 고분자를 제조하였으며, 이를 초고해상도 광학 현미경 중 하나인 SIM (structured illumination microscopy)를 통하여 확인하였다.

핵심용어 : 이중블록공중합체, 자기조립, 양자점, 형판 배열, 콜로이드 고분자

학번 : 2008-22739